Fractal branching organizations of Ediacaran rangeomorph fronds reveal a lost Proterozoic body plan

Jennifer Hoyal Cuthill[1] and Simon Conway Morris

Department of Earth Sciences, University of Cambridge, CB2 3EQ, UK.

[1]Correspondence to: jfh41@cam.ac.uk

The branching morphology of Ediacaran rangeomorph fronds has no exact counterpart in other complex macroorganisms. As such, these fossils pose major questions as to growth patterns, functional morphology, modes of feeding and adaptive optimality. Here, using parametric Lindenmayer systems, a first formal model of rangeomorph morphologies reveals a fractal body plan characterized by self-similar, axial, apical, alternate branching. Consequent morphological reconstruction for eleven taxa demonstrates an adaptive radiation based on three-dimensional space-filling strategies. The fractal body plan of rangeomorphs is shown to maximize surface area, consistent with diffusive nutrient uptake from the water column (osmotrophy). The enigmas of rangeomorph morphology, evolution and extinction are resolved by the realization that they were adaptively optimized for unique ecological and geochemical conditions in the late Proterozoic. Changes in ocean conditions associated with the Cambrian explosion sealed their fate.

Significance Statement

Rangeomorph fronds characterize the late Ediacaran Period (575-541 Ma), representing some of the earliest large organisms. As such, they offer key insights into the early evolution of multicellular eukaryotes. However, their extraordinary branching morphology differs from all other organisms and has proved highly enigmatic. Here, we provide a unified mathematical model of rangeomorph branching, allowing us to reconstruct 3D morphologies of eleven taxa and measure their functional properties. This reveals an adaptive radiation of fractal morphologies which maximized body surface area, consistent with diffusive nutrient uptake (osmotrophy). Rangeomorphs were adaptively optimal for the low-competition, high-nutrient conditions of Ediacaran oceans. With the Cambrian explosion in animal diversity (from 541 Ma), fundamental changes in ecological and geochemical conditions led to their extinction.

\body

In parallel with large-scale geochemical transitions associated with ocean oxygenation (1, 2, 3), the Ediacaran Period (635-541 Ma) records a major diversification of multicellular eukaryotes. Rangeomorph fronds (575-541 Ma) dominated early Ediacaran biotas (4) and have a characteristic branching morphology, distinct from any known Phanerozoic organism (5). Although the fronds are often preserved as flattened impressions, exceptional moldic fossils preserve details of the three-dimensional branching structure to a resolution of 30 μm (6). Qualitative classifications for rangeomorph branching patterns have been proposed (7, 8) but, importantly, no quantitative model has previously been formulated. Because branching is repeated over decreasing size scales (with up to four observed orders of branching) rangeomorph fronds have been informally described as self-similar and fractal (4, 5, 6). Although this has potential implications for the functional optimality of their morphologies (5, 9), the extent to which they are formally fractal and self-similar (10, 11) has not previously been tested. Furthermore, until now evolutionary transitions in branching patterns have not been characterized within any quantitative framework.

Rangeomorphs inhabited shallow to abyssal marine environments (1, 8, 12, 13, 14), evidently precluding photosynthesis for most taxa (12). Preservational features, including bending and over-folding (4, 15), suggest that rangeomorphs were soft-bodied. No evidence exists for either motility or active feeding (such as musculature, filter feeding organs or a mouth). Consequently, rangeomorphs have been reconstructed as sessile, feeding on organic carbon by diffusion (or possibly endocytosis) through the body surface (3, 5, 12, 16), with a large surface area to volume ratio aiding nutrient uptake (5, 16). The adaptive potential of their different branching morphologies has, however, never been quantified.

Here, using parametric Lindenmayer-systems (L-systems) (17, 18), we present a unified model to describe the branching structure of Ediacaran rangeomorph fronds. Our

quantitative parameters provide a far more detailed definition of frond morphology than was previously possible. These parameters are then used to reconstruct 3D space-filling strategies within the group and evaluate potential frond functions, revealing an adaptive radiation of fractal organizations. This provides a new framework for the study of growth, functional morphology and evolution of these 'lost constructions' (19).

Results and Discussion

Our L-system model comprises an initial axiom (starting branch segment), production rules for axial, apical, alternate branching and 28 parameters which together control branch production, elongation rates and three-dimensional branching angles (SI Appendix: Table S1). This incorporates both (sub-) apical branch production (distal extremities form the sites for subsequent branching) and expansion (branches grow in length and diameter throughout life), based on relative branch sizes and potential ontogenetic series (4, 7, 6, 20, 21). At each step in the axial branching process, an apical branch segment (e.g. the tip of the stem) produces one lateral branch segment (e.g. the beginning of a new primary lateral branch) and an additional axis segment (e.g. the new stem apex) (Fig. 1, SI Appendix: Videos S1-S3). Lateral branches are produced alternately (e.g. left then right) along a branch axis. Reconstruction of overall morphologies that closely match the anatomy of the fossils (Fig. 2, SI Appendix) validates this model of branching and growth. Collectively, these reconstructions demonstrate how different body shapes and symmetry patterns (characteristics employed by some previous studies (22, 23)) emerge from variations on a shared branching pattern. Resulting body organizations include alternate-symmetry (also known as glide-symmetry) in frontal view (superficially bilateral symmetry, off-set due to alternate branching on the right and left of an axis (7)), bilateral or tetraradial symmetry in apical view, and helical torsion around the main body axis (Fig. 3, SI Appendix).

Previous descriptions (following (6)) informally suggested that rangeomorphs possessed a shared fractal module consisting of a centimetre-scale, self-similar 'frondlet' (conceptually similar to the primary lateral branch and associated sub-branches, as formalized here). We demonstrate that rangeomorph morphologies can be reconstructed by applying approximately self-similar branch production rules (as described above) at increasingly fine scales, although these may be modified by different parameter values to give subtle variations in the level of self-similarity (SI Appendix: Table S1). These production rules apply across the branching system of the frond (sometimes called the 'petalodium' (8)), from the stem (the 0 order branch, which produces the 1st order lateral branches) to the highest order of branching (that is, from the 3rd order branches) (Fig. 1). This reveals that self-similarity extends beyond the frondlet, previously hypothesized to represent the basic modular unit (6). That is to say, the entire rangeomorph frond shows approximately self-similar branching, while the basic unit repeated throughout the frond is a cylindrical branch segment. This branch segment can be broadly related (6) to Seilacher's concept of the fractal "pneu" (24). We also show that rangeomorph fronds are approximately fractal (10) with non-integer fractal dimensions of 1.6 to 2.4 as determined by the 3D box counting method (SI Appendix: Fig. S13).

Shared possession of an approximately self-similar and fractal, axial, apical and alternate branching body plan supports a rangeomorph clade (Rangeomorpha, Pflug, 1972 cited in (8)) but significantly increases the range of diagnostic characters (previously restricted to repeated fine-scale branching (8) only visible in exceptionally preserved specimens). Note that this rangeomorph body plan does not extend to other enigmatic Ediacaran macroorganisms, such as *Swartpuntia*, *Ernietta* (8) or *Dickinsonia* (23). This suggests that the rangeomorphs were a distinct, high ranking clade of multicellular

eukaryotes (2, 6) and supports the view that the Ediacaran biota was far from homogenous, but instead included diverse phylogenetic lineages and body plans (25).

More widely, approximately analogous morphologies (including alternate, axial and apical to sub-apical branching patterns) are seen across the tree of life, among bacteria, protists, plants, fungi and animals, so indicating extensive convergent evolution of fractal-like branching structures (26). Therefore, superficially similar branching arrangements are not necessarily indicative of close phylogenetic affinity. Indeed, one of the most striking features of such fractal patterns is that highly detailed structures can be described mathematically by quite simple rules (27). Correspondingly, the genetic and developmental programs of self-similar biological structures may be comparatively simple (and conceivably require a relatively small number of genetic changes to evolve), because emergent structural properties do not, in themselves, require genetic specification (9, 11, 28).

While some exceptional rangeomorph fossils do preserve aspects of three-dimensional morphology (4), the nature of these casts means that the full depth of the frond (perpendicular to the preserved surface) cannot be measured directly (21). However, our reconstructions of three-dimensional branching patterns provide estimates of overall dimensions (Fig. 3), throwing new light on frond ecology. This also allows much more realistic estimates of frond surface area and volume than were possible using simple geometric models (5, 16).

Ratios of external surface area to tissue volume (assuming a 0.1 mm thick metabolic tissue layer (5)) fall between 77 and 352 cm^2/cm^3 (SI Appendix: Table S2), within the range for osmotrophic giant bacteria (see also (5)). Absolute surface areas (SI Appendix: Table S2) also reach very high values. For example, in the large recliner *Hapsidophyllas flexibilis* the external surface area is equivalent to 58 m^2 (in the same order of magnitude as the human lung). Given their large size, rangeomorphs almost certainly relied upon aerobic metabolism

(29) of organic carbon (3, 5). Among the eleven studied taxa, the vast majority of body surface area (> 95%) is provided by the branching frond (rather than the buried holdfast, where present), and this would have maximized access to the water column. Thus, rangeomorphs most likely fed by the uptake of dissolved organic carbon (5) (or possibly small organic particles (3)), as well as oxygen, from the surrounding seawater, primarily through the surface of the branching frond (although subsidiary nutrient capture from the sediment, through the holdfast or reclining body surface, is a possibility (16, 23)).

The fractal branching of the rangeomorph frond is an optimal geometric solution to the problem of space-filling, maximizing surface area (and correspondingly nutrient uptake) within the boundaries of the total space occupied (9). The most planar of the fronds have fractal dimensions that range from 1.6 (for *Avalofractus*) to just below 2 (at 1.99 for *Trepassia*), as estimated by 3D box counting (SI Appendix: Fig. S13). Other taxa (*Beothukis, Bradgatia*, *Culmofrons* and *Fractofusus andersoni*) have estimated fractal dimensions above 2 (up to 2.4 for *Bradgatia*, SI Appendix: Fig. S13), reflecting branch arrangements which provide greater 3D space-filling. For example, the helical ("lettuce" like (32)) arrangement of the primary branches in *Bradgatia* (Fig. 3, SI Appendix) occupies the greatest relative bounding volume (SI Appendix: Table S2) and achieves the highest fractal dimension. Space-filling by the "skeleton" of the rangeomorph branching frond (composed of 1D branch segments) is, therefore, so effective that its dimension approaches (or even exceeds) that of a 2D plane. In contrast to a simple plane (that is, an ellipse of comparable height and width), however, the branching frond provides up to 40 times the external surface area (SI Appendix: Table S2). Such structures (incorporating dense, planar feeding nets) maximize nutrient capture, particularly if oriented (passively or actively) with the width axis of a feeding net perpendicular to the ambient water current (30).

Cluster analysis of the total three-dimensional space occupied by a representative of each taxon (Fig. 3, SI Appendix: Fig. S12) suggests diversification into three major space-filling strategies: those maximizing vertical height (Fig. 3, blue), those of more moderate height including some with high volume (green), and inferred benthic recliners with an accentuated horizontal width (red). Given that the greatest variance between taxa is in height rather than width or depth (Fig. 3, SI Appendix: Table S2), this suggests ecological tiering (31) and a strong selective pressure for greater height. The fluid dynamics that rangeomorphs experienced are likely to have depended on their local density and size, with a recent theoretical fluid flow model suggesting that dense rangeomorph communities may have created specific canopy flow conditions (16). This model predicts a strong selective advantage for increased height to maximise access to faster flowing fluid, thereby increasing nutrient absoption.

Our growth model also reveals a range of mechanisms by which modifications to a shared growth pattern can achieve different space-filling strategies (Fig. 3, SI Appendix: Table S1). For example, height can be favored via rapid production of primary branches at angles relatively close to vertical (e.g. *Charnia masoni*) or by a high rate of elongation for the basal stem segment (e.g. *Culmofrons plumosa*). To increase frond width, primary branches are produced at a less acute angle from the stem (e.g. *Beothukis*, *Bradgatia*). Space-filling of the 3rd dimension (i.e. adding depth if vertically oriented or height if horizontal, Fig. 3) may also be augmented, by the helical arrangement of the primary branches around the central axis (e.g. *Beothukis* (4), *Bradgatia* (32)), by rotations of the primary branches to form a double layered structure (e.g. *Fractofusus* (15)), or via primary branch curvature (e.g. *Hapsidophyllas*).

Some of the tallest rangeomorphs (*Charnia* and *Trepassia*) appear in the oldest part of the Avalonian sequence (1, 4). As it stands, this suggests that fronds maximizing vertical

height evolved first, followed by diversification into a wider range of three-dimensional branching and space-filling strategies (Fig. 3). However, it is possible that these large rangeomorphs (with *Trepassia* reaching more than 1m in length (1, 4)) had smaller, and as yet unknown, precursors. Further to this, evolutionary transitions within the Rangeomorpha should be interpreted with some caution due to uncertainties regarding true paleobiogeographic and temporal ranges (SI Appendix: Table S3) (13).

Among the *in situ* communities of the earliest, Avalon Assemblage, rangeomorphs are by far the most diverse and abundant macroorganisms (33). Furthermore, establishment of the major rangeomorph space-filling strategies (Fig. 3) preceded the appearance of a much wider range of macroorganisms (such as Dickinsoniomorphs and Erniettomorphs) in the White Sea Assemblage from approximately 555 Ma (34), with all included rangeomorphs except *Rangea* itself (35) first appearing in the Avalon Assemblage, by 565 Ma (SI Appendix: Table S3). This suggests that early diversification of rangeomorph branching patterns effected a radiation in the key characters of body size and microhabitat (which are linked by the interaction between body size and access to fluid flow (16, 33)) and was driven by ecological competition between rangeomorph taxa. These features are consistent with a rapid adaptive radiation shortly after the Gaskiers glaciation (from 579 Ma (1, 4)). Thus, evolution of the fractal branching morphology achieved unprecedented body size and elevated the rangeomorphs into the new ecological realms of the water column, enabling diversification in an environment more or less free of other macroorganisms.

Conclusions

With their terminal Proterozoic extinction and unique morphology, Ediacaran rangeomorph fronds have been described as a ‘failed experiment’ (24). However, our analysis demonstrates that these intriguing fossils possessed a fractal morphology which combined

programmatic (and potentially genetic-developmental (9, 11, 28)) simplicity, structural versatility and functional optimality for the uptake of organic carbon (osmotrophy) and oxygen. The appearance of rangeomorph fossils (1) occurred after a move away from anoxic, sulfidic and ferruginous oceans, towards conditions more favorable for aerobic macroorganisms (2, 29). Their disappearance coincides with the Cambrian explosion in metazoan diversity, a dramatic increase in competition and, crucially, decreased availability of organic carbon in ocean water (2, 12, 19, 24, 34, 36). These potentially interacting factors suggest that the Ediacaran to Cambrian transition was a bad time to be a sessile, soft-bodied osmotroph. The unique rangeomorph fronds were fractal, surface area specialists of the Ediacaran. At the Cambrian explosion, the ecological and geochemical conditions for which the rangeomorphs were optimized ceased to exist, and their extraordinary body plan was lost from life's repertoire.

Methods

First, this study established a unified model for rangeomorph theoretical morphology using parametric (18) Lindenmayer (L) systems (17), written within the L-studio programming environment (37). L-systems are a class of parallel derivation grammar, in which specified production rules are applied in parallel to control iterative rewriting of the axiom (a starting string, here representing the first stem segments, and holdfast if present). The symbols produced are then interpreted graphically to visualize a geometry encoded by the output L-system string (representing the branching system) (18). A branching L-system is characteristically fractal, with self-similar elements visible at decreasing size scales (38). Importantly, *parametric* L-systems allow branching parameter values (such as branching angles and growth rates) to vary between branches (for example of different orders or ages),

enabling realistic representation of biological structures with non-uniform branching patterns (18).

Rangeomorph morphologies were modelled using formal production rules and parameters based on branching patterns of eleven studied species and quantitative measurements (of branching angles and body dimensions) from best-preserved representatives (SI Appendix). For each species, the L-system output geometry was then processed and analyzed using Blender 2.69 and Matlab (2012b, Mathworks). For measurement comparability, L-system output was standardized to the same finite approximation (four orders of branching).

The fractal dimension of each modelled frond was estimated using box counting, the method most commonly used to analyze complex fractal shapes (10). This method determines the number (n) of boxes of a given size (r) that cover the input image. The scale (r) is incrementally decreased to determine the relationship between box size and image coverage. The slope of the line for this relationship gives the fractal dimension of the image $D = -(\log(n)/\log(r))$. If dimension D is not an integer, this indicates that the image is a fractal (its geometry does not correspond exactly to an integer dimension i.e. a 1D line, 2D plane or 3D volume). The input image for 2D box counting was a 2D binary (black or white) skeleton of the branching pattern, in frontal view (SI Appendix: Fig. S13). Input for 3D box counting was a 3D binary skeleton of the branching pattern (SI Appendix: Fig. S13). 2D box counting was conducted using ImageJ (39). 3D box counting was conducted in Matlab with a script incorporating the Wavefront OBJ toolbox (40), Inhull function (41) and boxcount toolbox (42). Because 3D box counting is highly computationally intensive, two large species *Fractofusus misrai* and *Pectinifrons abysallis* were analyzed using 2D box counting only.

Functionally relevant frond properties were calculated from the output mesh, including the surface area to tissue volume ratio (with modelled tissue depths of 0.1, 0.5, and

1mm (comparable to (5)), and the size (height, width, depth) of a bounding box around the frond. Bounding box axes for each species were oriented relative to inferred life position (based on fossil morphology and preservation). Dimensions for each species were scaled based on approximate specimen lengths recorded in the literature (SI Appendix: Table S2). A Euclidean cluster analysis of these scaled dimensions was conducted using paired group linkage in PAST (43).

Acknowledgements. We thank A. Liu, J. Gehling, C. Kenchington, and M. D. Brasier for discussion and making fossil casts and photographs available for study, with additional thanks to the Oxford University Museum of Natural History and the University of Cambridge Sedgwick Museum of Earth Sciences for access to their collections and to the South Australia Museum for providing specimen photographs. We also thank S. Gerber and three anonymous reviewers for highly constructive comments on the manuscript. This research was supported by Templeton World Charity Foundation grant LBAG/143.

References

1. Narbonne GM, Gehling JG (2003) Life after snowball: the oldest complex Ediacaran fossils. *Geology* 31:27-30.

2. Narbonne G (2010) Ocean chemistry and early animals. *Science* 328:53-54.

3. Knoll AH (2011) The multiple origins of complex multicellularity. *Annu Rev Earth Planet Sci* 39:217-239.

4. Narbonne GM, Laflamme M, Greentree C, Trusler P (2009) Reconstructing a lost world: Ediacaran rangeomorphs from Spaniard's Bay, Newfoundland. *J Paleont* 83:503-523.

5. Laflamme M, Xiao S, Kowalewski M (2009) Osmotrophy in modular Ediacara organisms. *Proc Natl Acad Sci USA* 106:14438-14443.

6. Narbonne G (2004) Modular construction of Early Ediacaran complex life forms. *Science* 305:1141-1144.

7. Brasier M, Antcliffe JB, Liu AG (2012) The architecture of Ediacaran fronds. *Palaeontology* 55:1105-1124.

8. Laflamme M, Narbonne GM (2008) Ediacaran fronds. *Palaeogeogr Palaeoclimatol Palaeoecol* 258:162-179.

9. Prusinkiewicz P, Barbier de Reuille P (2010) Constraints of space in plant development. *J Exp Bot* 61:2117-2129.

10. Mishra J, Mishra S (2007) *L-system fractals* (Elsevier Science & Technology, Amsterdam).

11. Ferraro P, Godin C, Prusinkiewicz P (2005) Toward a quantification of self-similarity in plants. *Fractals* 13:91-109.

12. Sperling EA, Peterson KJ, Laflamme M (2011) Rangeomorphs, *Thectardis* (Porifera?) and dissolved organic carbon in the Ediacaran oceans. *Geobiology* 9:24-33.

13. Gehling JG, Droser ML (2013) How well do fossil assemblages of the Ediacaran biota tell time? *Geology* 41:447-450.

14. Chen, Z, et al. (2014) New Ediacara fossils preserved in marine limestone and their ecological implications. *Scientific Reports* 4.

15. Gehling JG, Narbonne GM (2007) Spindle-shaped Ediacara fossils from the Mistaken Point assemblage, Avalon Zone, Newfoundland. *Can J Earth Sci* 44:367-387.

16. Ghisalberti M, et al. (2014) Canopy flow analysis reveals the advantage of size in the oldest communities of multicellular eukaryotes. *Curr Biol* 24:305-309.

17. Lindenmayer A (1968) Mathematical models for cellular interactions in development, parts I and II. *J Theor Biol* 18:280-315.

18. Prusinkiewicz P, Hanan J (1990) Visualization of botanical structures and processes using parametric L-systems. *Scientific visualization and graphics simulation*, ed. Thalmann, D (Wiley & Sons), pp 183-201.

19. Seilacher A (1992) Vendobionta and Psammocorallia: lost constructions of Precambrian evolution. *J Geol Soc London* 149:607-613.

20. Liu AG, Mcllroy D, Mathews JJ, Brasier MD (2013) Exploring an Ediacaran 'nursery': growth, ecology and evolution in a rangeomorph palaeocommunity. *Geol Today* 29:23-26.

21. Laflamme, M. et al. (2007) Morphology and taphonomy of an Ediacaran frond: *Charnia* from the Avalon Peninsula of Newfoundland. *Geol Soc London Spec Publ* 286: 237-257.

22. Shen B, Dong L, Xiao S, Kowalewski M (2008) The Avalon explosion: evolution of Ediacara morphospace. *Science* 319:81-84.

23. Dzik J (2003) Anatomical information content in the Ediacaran fossils and their posssible zoological affinities. *Integr Comp Biol* 43:114-126.

24. Seilacher A (1989) Vendozoa: organismic construction in the Proterozoic biosphere. *Lethaia* 22:229-239.

25. Xiao S, Laflamme M (2008) On the eve of animal radiation: phylogeny, ecology and evolution of the Ediacara biota. *Trends Ecol Evol* 24:31-40.

26. Kaandorp JA, Kübler JE (2001) *The algorithmic beauty of seaweeds, sponges and corals* (Springer-Verlag, Berlin).

27. Mandelbrot BB (1977) *The fractal geometry of nature* (Freeman and Company, New York).

28. Narbonne GM (2005) The Ediacara biota: Neoproterozoic origin of animals and their ecosystems. *Annu Rev Earth Planet Sci* 33:421-442.

29. Catling DC, Glein CR, Zahnle KJ, McKay CP (2005) Why O_2 is required by complex life on habitable planets and the concept of planetary "oxygenation time". *Astrobiology* 5:415-437.

30. Singer A, Plotnick R, Laflamme M (2012) Experimental fluid mechanics of an Ediacaran frond. *Palaeont Electron* 15:19A.

31. Clapham ME, Narbonne GM (2002) Ediacaran epifaunal tiering. *Geology* 30:627-630.

32. Flude LI, Narbonne GM (2008) Taphonomy and ontogeny of a multibranched Ediacaran fossil: *Bradgatia* from the Avalon Peninsula of Newfoundland. *Can J Earth Sci* 45:1095-1109.

33. Laflamme M, Flude LI, Narbonne G (2012) Ecological tiering and the evolution of a stem: the oldest stemmed frond from the Ediacaran of Newfoundland. *J Paleontol* 86:193-200.

34. Laflamme M, et al. (2013) The end of the Ediacaran biota: extinction, biotic replacement, or Cheshire cat? *Gondwana Res* 23:558-573.

35. Vickers-Rich, et al. (2013) Reconstructing *Rangea*: new discoveries from the Ediacaran of Southern Namibia. *J Paleontol* 87:1-15.

36. Butterfield NJ (2009) Oxygen, animals and oceanic ventilation: an alternative view. *Geobiology* 7:1-7.

37. Prusinkiewicz P, Karwowski R, Mech R, Hanan J (2000) L-studio/cpfg: A software system for modeling plants. *Applications of Graph Transformations with Industrial Relevance* (Springer), pp. 457-464.

38. Zamir M (2001) Arterial branching within the confines of fractal L-system formalism. *J Gen Physiol* 118:267-275.

39. Schneider CA, Rasband WS, Eliceiri KW (2012) NIH Image to ImageJ: 25 years of image analysis. *Nature Methods* 9:671-675.

40. Kroon DJ (2011) Wavefront OBJ toolbox. *MATLAB Central File Exchange.*

41. D'Errico J (2012) Inhull. *MATLAB Central File Exchange.*

42. Moisy F (2008) Boxcount. *MATLAB Central File Exchange.*

43. Hammer Ø, Harper DAT, Ryan PD (2001) PAST: Paleontological Statistics Software Package for Education and Data Analysis. *Palaeontol Electron* 4:9.

44. Nedin C, Jenkins RJF (1998) First occurrence of the Ediacaran fossil *Charnia* from the southern hemisphere. *Alcheringa* 22:315-316.

Figure Legends

Fig. 1. Schematic L-system model of *Beothukis mistakensis*. (*A*) First 3 steps of the branching process. (*B*) Final morphology at step 38. Segment colors indicate relative age, from oldest (red) to youngest (light blue). Numbers indicate branch order (0 stem, 1 primary, 2 secondary, 3 tertiary, 4 quaternary).

Fig. 2. Ediacaran rangeomorph fossils and their three-dimensional L-system models. (*A-B*) *Avalofractus abaculus. A* reproduced with permission from (4) Fig. 3.1. (*C-D*) *Charnia masoni*. (*C*) South Australia Museum specimen number P36574, described in ref. 44, image courtesy of Jim Gehling (South Australia Museum, Adelaide, Australia). Scale bars 1cm.

Fig. 3. Three-dimensional space-filling by Ediacaran rangeomorph fronds (illustrated 1/2 estimated life size). Locations indicate estimated bounding box size in inferred life orientation (values SI Appendix: Table S2). Frond colors indicate Euclidean distance-based clusters (cophenetic correlation coefficient = 0.77).

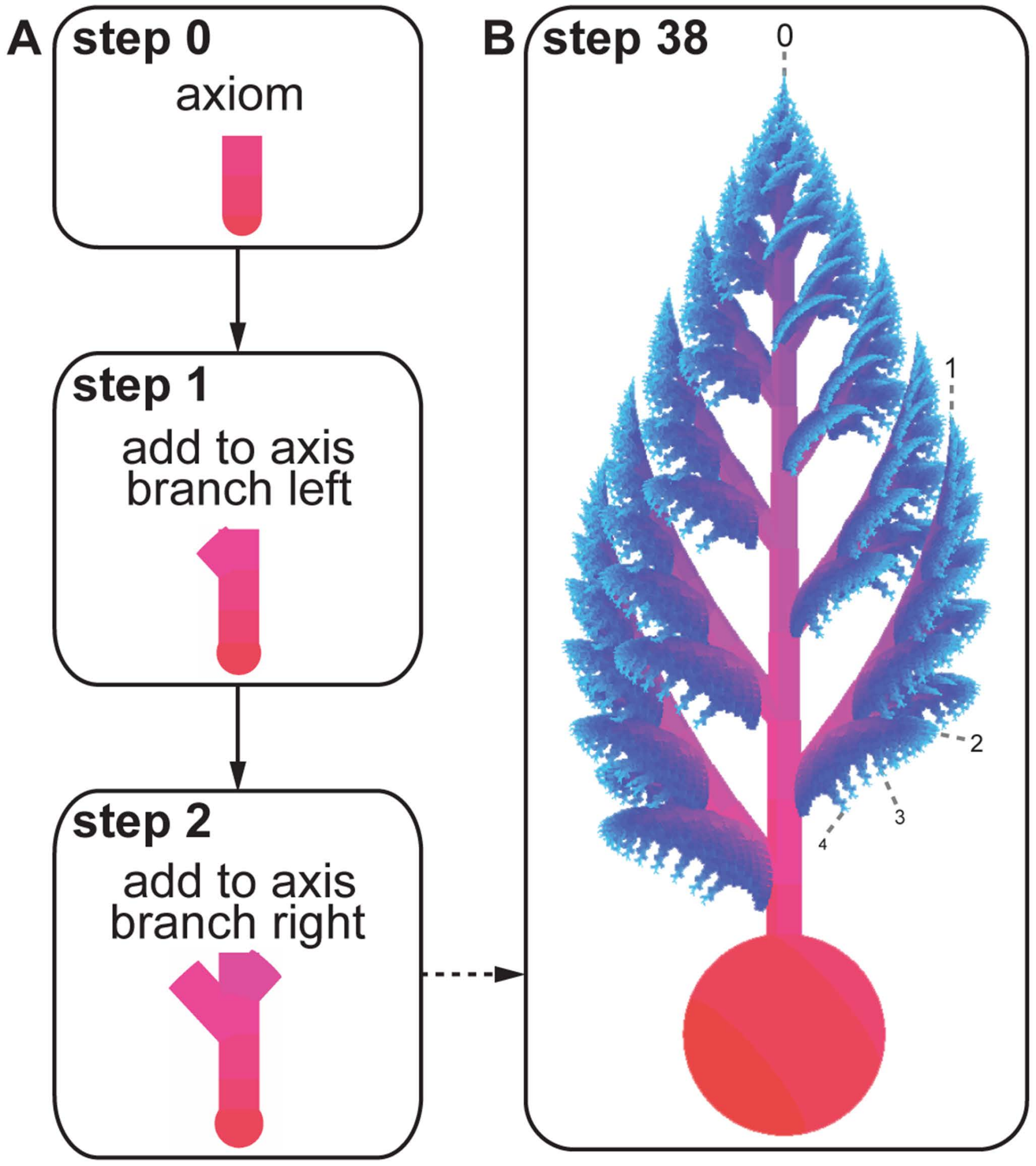
A
step 0
axiom
step 1
add to axis
branch left
step 2
add to axis
branch right
B
step 38
0
1
2
3
4

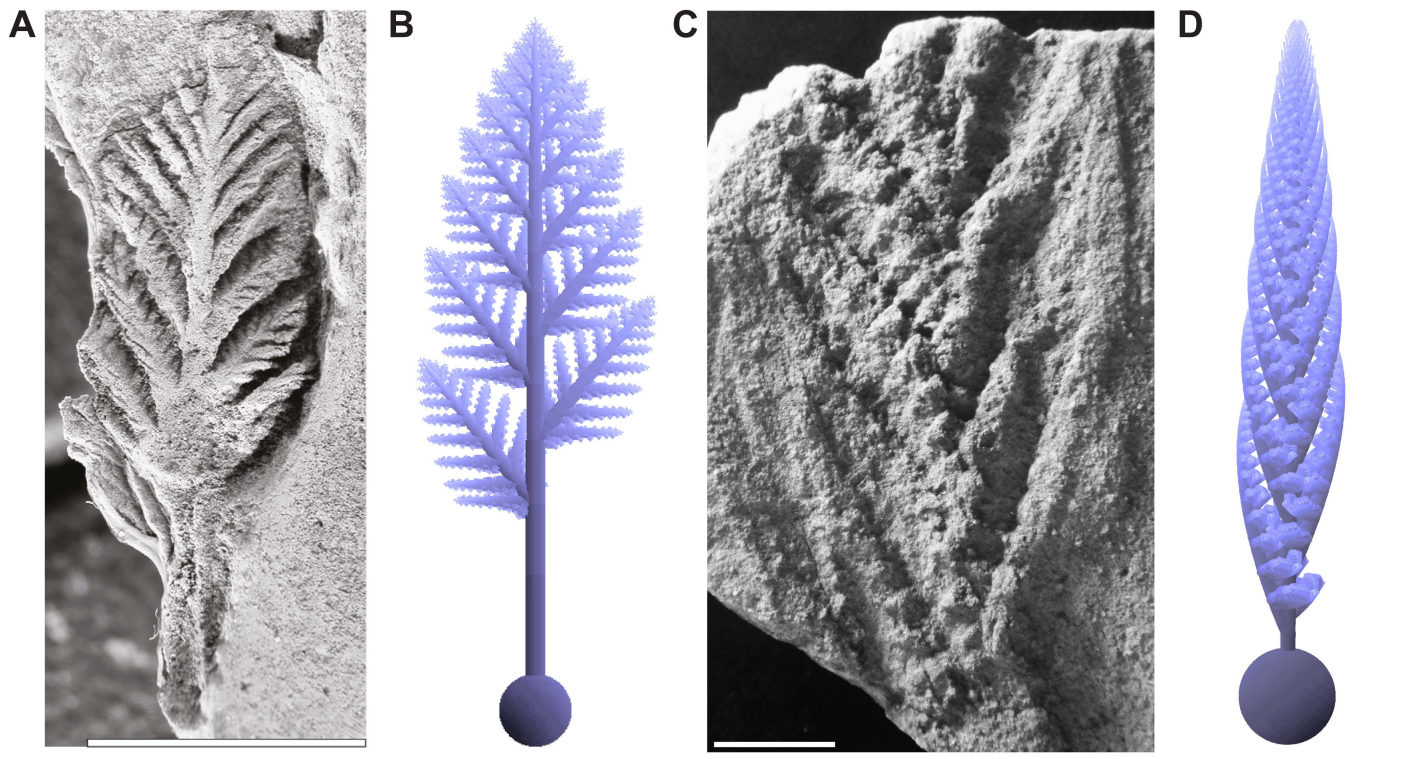
A
B
C
D

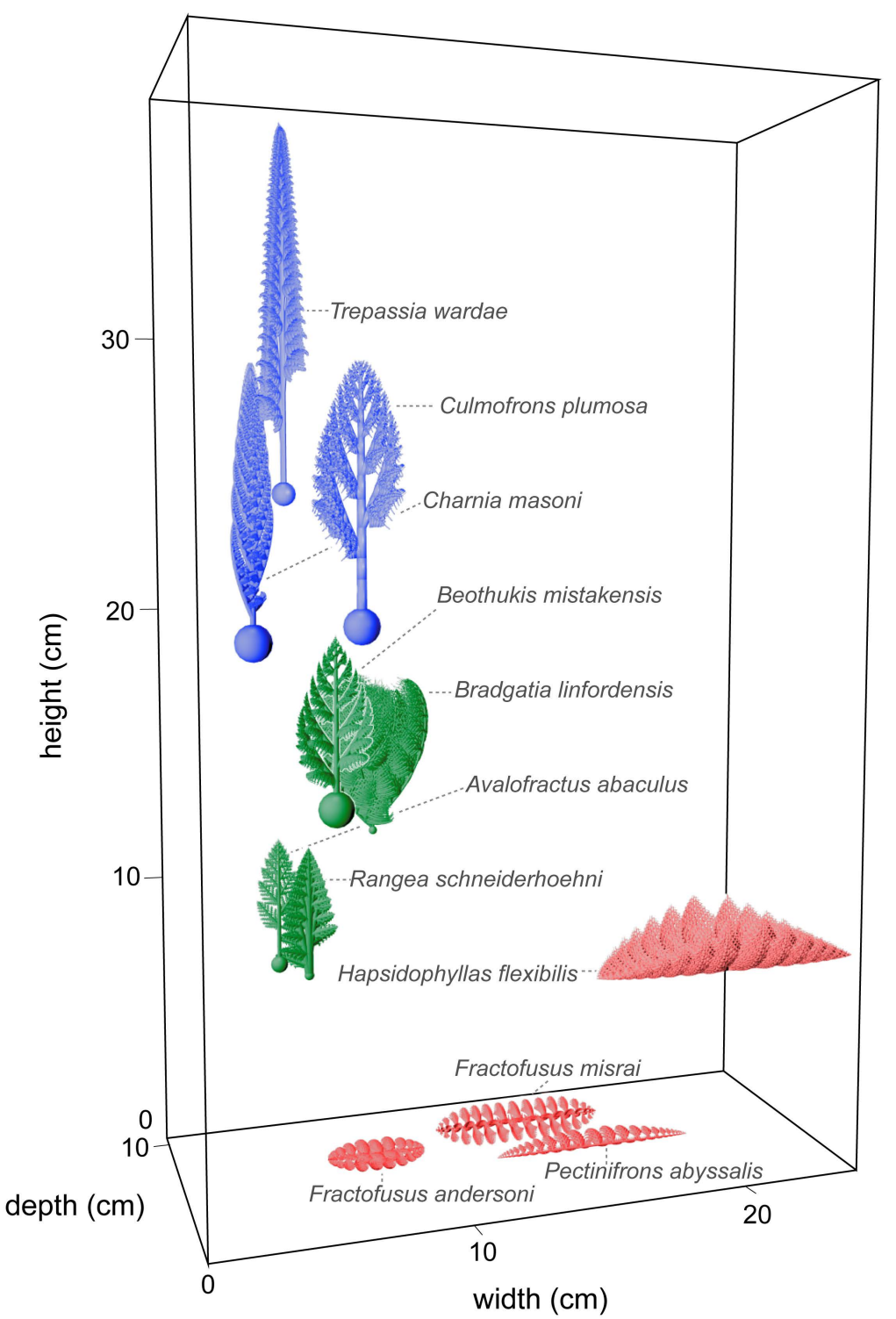
Trepassia wardae
Culmofrons plumosa
Charnia masoni
Beothukis mistakensis
Bradgatia linfordensis
Avalofractus abaculus
Rangea schneiderhoehni
Hapsidophyllas flexibilis
Fractofusus misrai
Pectinifrons abyssalis
Fractofusus andersoni
height (cm)
30
20
10
0
depth (cm)
10
0
0
10
20
width (cm)

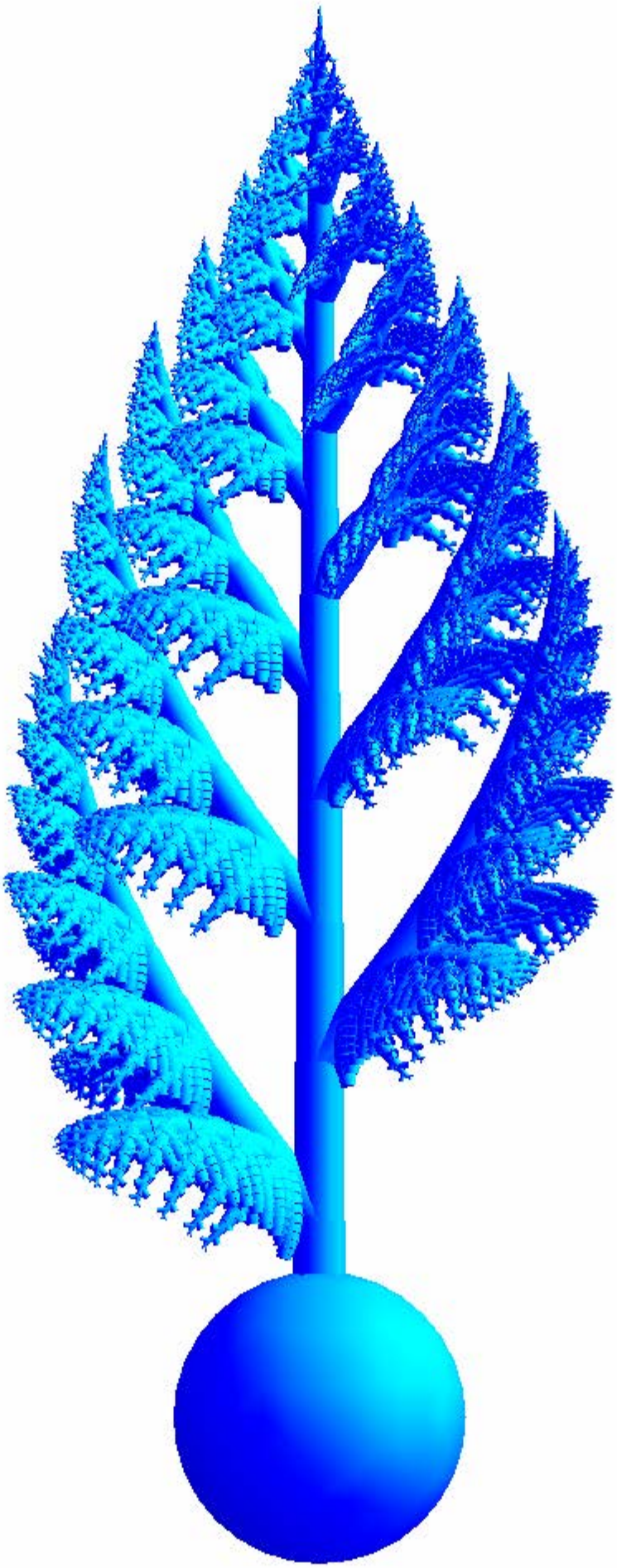

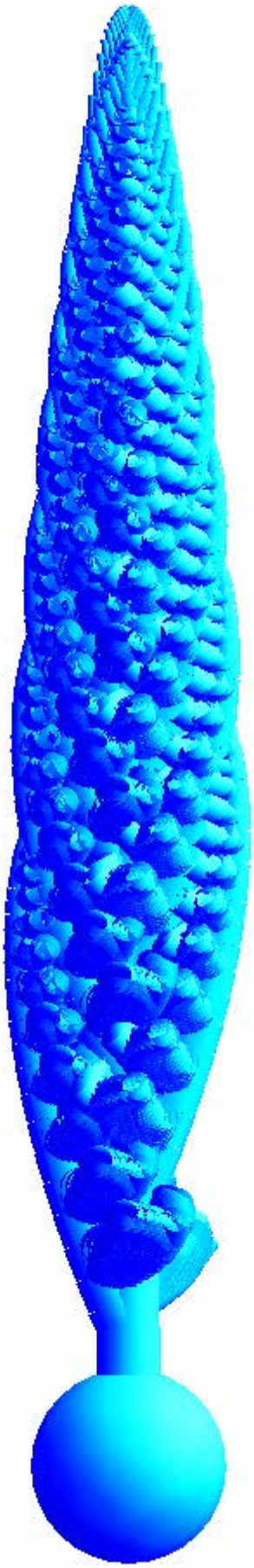

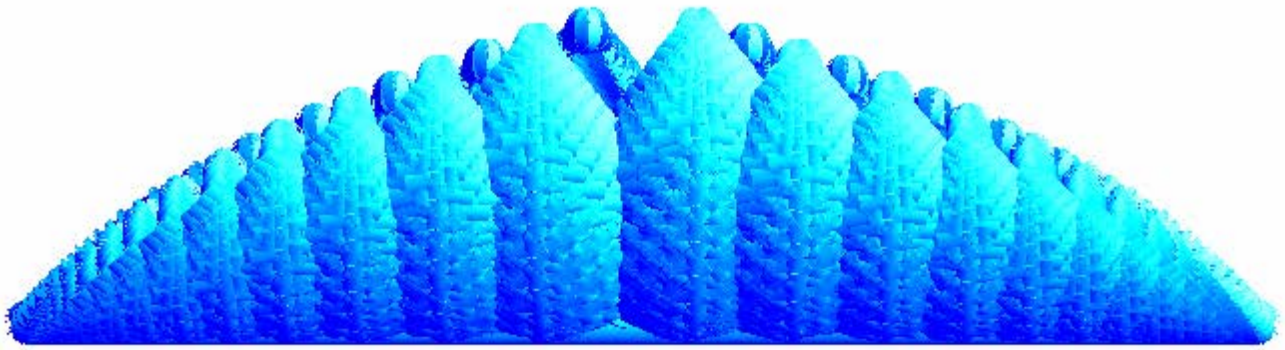

SI Appendix

Specimen analysis for L-system parameter coding

Avalofractus abaculus

Alternate, self-similar branching is visible in exceptionally preserved, three-dimensional specimens from Spaniard's Bay, Newfoundland, described by Narbonne et al. (4). Measurements taken from Fig. 3.1 of Narbonne et al. (4) were used to code y-axis branching angles for the 1st order branches (n=16 measurements gave a mean of 38°) and 2nd order branches (mean=47°, n=24). Preservation and photographic image resolution are not sufficient to allow measurement of branching angles for branches of order greater than 2. In the absence of evidence to the contrary, branches of order ≥ 3 were coded as having y-axis branching angles self-similar to those of 2nd order branches. An x-axis rotation of 15° was used to model pivoting (4) of the branches relative to their axis. The frond shape is ovate (4), with width approximately 47% of height (excluding basal stem and holdfast). Specimens preserve between four and eight imbricate primary (1st order) branches on left and right sides of the main stem (4). These interrelated morphological features were modeled using a moderate lateral branching delay and a moderate increase in lateral branch elongation rate, relative to the stem (see Table S1 for parameter values). The imprint of a bulbous holdfast (modeled as a sphere) is visible in one specimen (Fig. S1*D*; Fig. 3.4 of (4)). Holdfast diameter measured from this specimen is approximately 38% of maximum frond width.

Fig. S1. *Avalofractus abaculus*. (*A*) Specimen from Spaniard's Bay, Newfoundland. Image reproduced with permission from Narbonne et al. (4) Fig. 3.1. Scale bar 1cm. (*B*) L-system model. Frontal view. Colors indicate increasing branch segment age from base to apices. (*C*) Rotated view. (*D*) Image reproduced with permission from Narbonne et al. (4) Fig. 3.4. Scale bar 1cm.

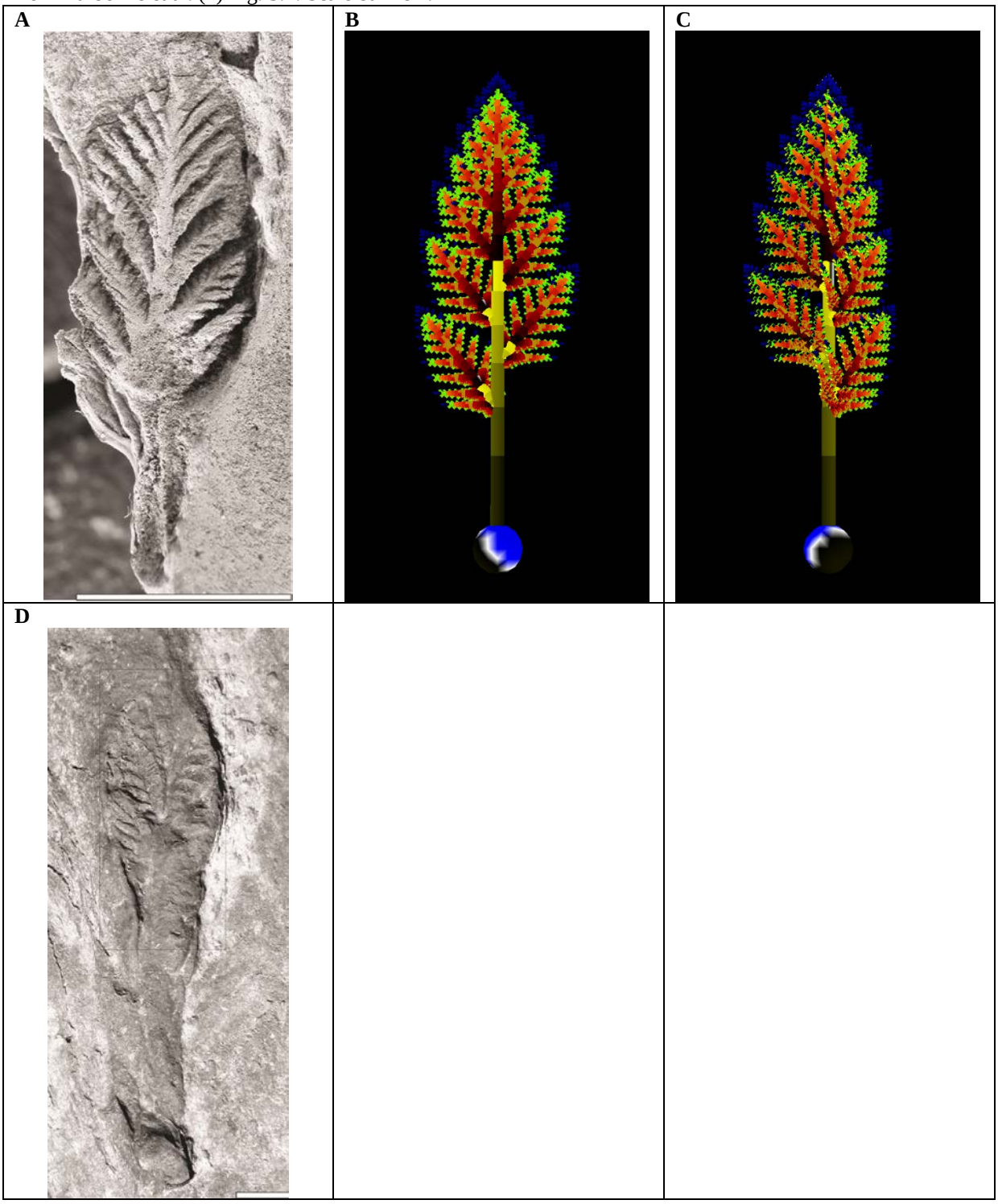

Beothukis mistakensis

Primary branches are visibly alternating. However, secondary (2nd order) branches are only visible on one side of each primary branch. This has been interpreted as the probable result of "folding" (4) or "furling" (45) of secondary branches over the primary branch axis so that one side of an alternating series is "undisplayed" (45). Here, this feature was modeled using a 90° z-axis rotation of the primary branches accompanied by a 5° x-axis curvature for branches of order ≥ 2 (giving a convex upper surface to the secondary branches). A concave upper curvature to the primary branches is visible in the exceptionally preserved specimen from Spaniard's Bay (Fig. S2*A*; Narbonne et al. (4) Fig. 5.1). This was modeled using 357° x-axis curvature. Y-axis branching angles were coded based on measurements from Fig. 5.1 of Narbonne et al. (4) (1st order mean=43, n=10; 2nd order mean=46, n=10; 3rd order mean=56, n=15 used for branches order ≥ 3). A small amount of helical torsion of the stem (reported to be visible in multiple specimens (4)) was modeled using a 355° z-axis rotation (branch order 0 only). Six to nine primary branches may be visible on each side of a frond (4) and frond width was measured at approximately 54% of height. This morphology was modeled using a moderate lateral branching delay and moderate increase in lateral branch elongation rate relative to the stem (Table S1). Holdfast width was measured at approximately 64% of maximum frond width.

Fig. S2. *Beothukis mistakensis.* (*A*) Specimen from Spaniard's Bay, Newfoundland. Image reproduced with permission from Narbonne et al. (4) Fig. 5.1. Scale bar 1cm. (*B*) L-system model. Frontal view. (*C*) Rotated view.

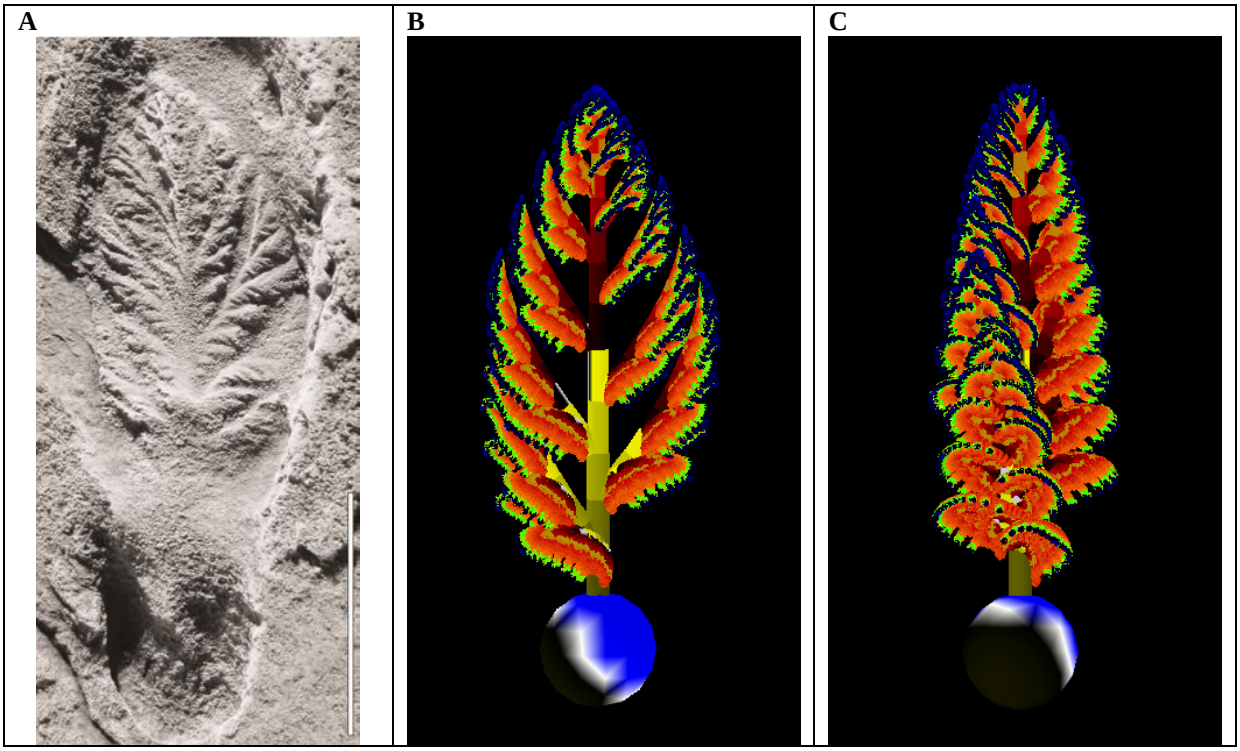

Bradgatia linfordensis

This species is known from multiple specimens from Leicestershire (Boynton & Ford, 1995 cited in (32)) and Newfoundland and has been variously described as fan (45), bush, leek, or lettuce shaped (32). Small (likely juvenile) and exceptionally preserved specimens from Spaniard's Bay, Newfoundland (32) suggest that long branches (labelled as primary branches in the ordering series used here) emerge at close intervals from the basal region (Fig. S3*A-B*), with three to eight usually visible in fossil specimens (32). This arrangement is

modeled here using a very reduced elongation rate (Table S1) for the central axis, from which the primary branches emerge (Fig. S3*D-E*). Specimens show a variety of dimensions, from height greater than width (Fig. S3) to width greater than height (e.g. (32). Fig. 3), suggesting ontogenetic and taphonomic variability (32). Further to this, some specimens appear to have been flattened on their side (with the basal main axis at the bottom of the specimen, as in Fig. S3*A-C*, with specimen Fig. S3*C* having width approx. 66% of height), while others appear to have flattened from above, with the primary branches emanating from a central region (32). This second taphonomic class suggests that the large branches radiated from the center, through 360° (32). Here, the distribution of the primary branches is modeled using a 42.5° helical z-axis rotation around the central axis. This results in a 137.5° spacing between sequentially produced primary branches, a common natural pattern which maximizes the distance between helically distributed structures (46). The small, exceptionally preserved specimens of Spaniard's Bay (Fig. S3*A-B*) show very elongate primary branches, with relatively evenly sized and spaced, diamond-shaped secondary branches. The secondary branches have a moderate, convex upper curvature (Table S1). Large, presumably adult specimens from Leicestershire (e.g. Fig. S3*C*) also show elongate, plumose primary branches although fine details are not as well preserved. This specimen indicates a moderate concave upper curvature to the primary branches (Table S1). The plumose morphology of the primary branches was modeled using relatively low elongation rates, plus growth functions which suppress the relative growth of older branches, for branches of order ≥ 2 (Table S1). Three-dimensionally preserved specimens indicate the presence of a small, spherical, basal holdfast (32).

Fig. S3. ***Bradgatia linfordensis.*** (*A*). Image reproduced with permission from Flude & Narbonne (32) Fig. 4*A*. (*B*). Image reproduced with permission from Flude & Narbonne (32) Fig. 4*E*. © Canadian Science Publishing or its licensors. (*C*) British Geological Survey cast (specimen number GSM 105873) from the Bradgate Formation, Leicestershire, UK, held in the Sedgwick Museum of Earth Sciences, Cambridge. Scale bars 1cm. (*D*) L-system model. Frontal view. (*E*) Rotated (apical) view.

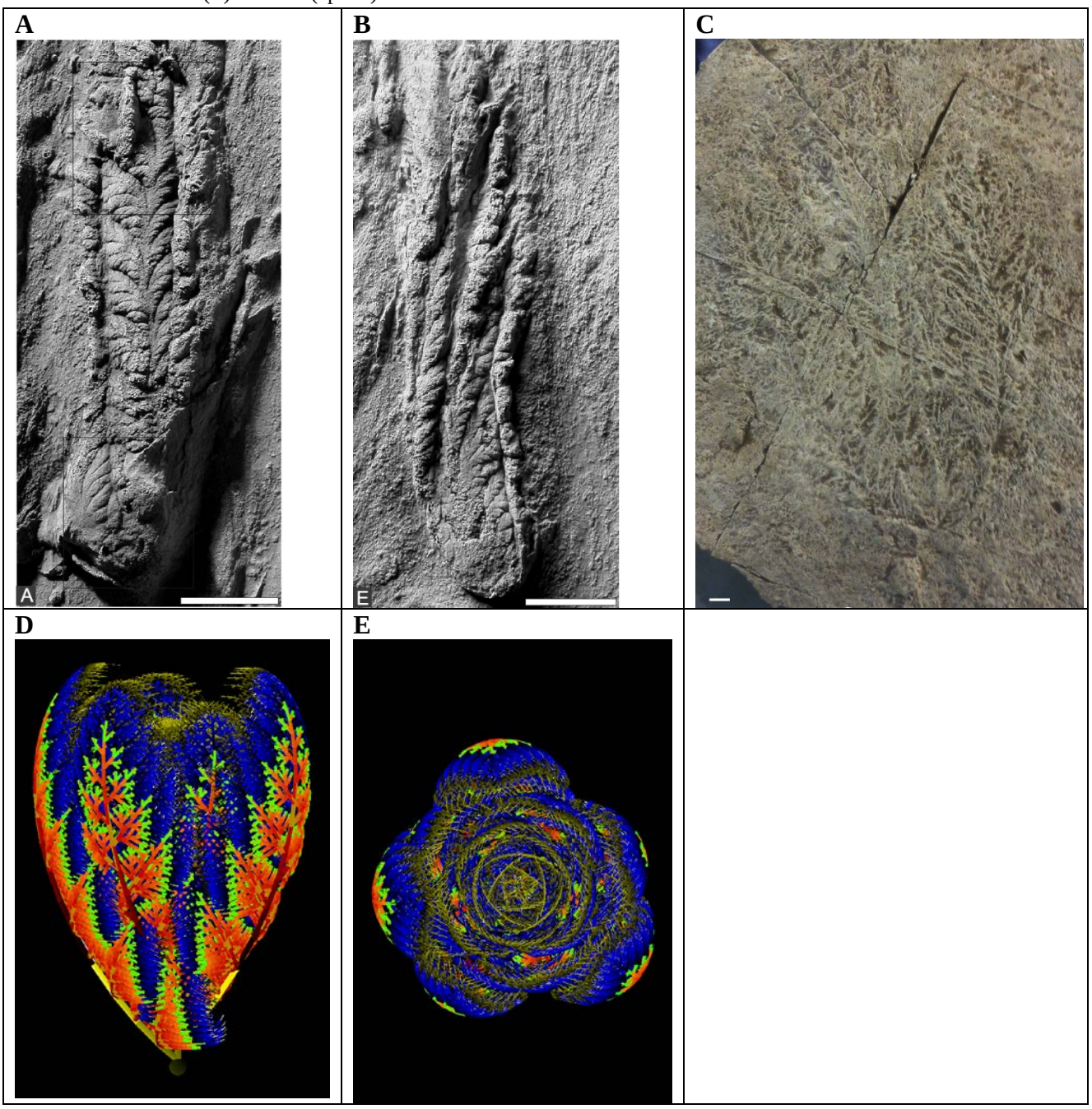

Charnia masoni

This species has regular, tightly packed alternating branches, emanating from an inferred central stem (21). Many specimens do not preserve branching structure beyond the primary branches. However, some exceptionally preserved specimens show self-similar, rangeomorph branching to 4 orders (e.g. (47) Fig. 2*B*). Secondary branches are visible only on one side of each primary branch in frontal view (4, 45). This is interpreted as the result of rotation of branches in an alternating series (4, 45). The close packing of primary branches makes it difficult to determine the origin and orientation of the 2nd order branches in many

specimens. However, a number of features suggest growth of 2nd order branches upwards from the primary branch (with 2nd order branch apices oriented towards the top of the frond). First, this is compatible with the widely noted zig-zag midline (e.g. Fig. S4*A*) here interpreted to result from stacking of the primary branches, so that the base of each 1st order branch (with its associated sub-branches) crosses over the stem and the lower part of the primary branch immediately above it. Second, this is supported by the fine-scale structure of exceptionally preserved specimens, such as that shown in Fig. S4*A*. In this specimen the free apices of the 2nd order branches appear to overlap upwards onto the branches above. In the lower part of this specimen, visible 3rd order branches also appear to be oriented apex-up. This branching architecture was modeled using a 270° z-axis rotation for the primary branches with 26° y-angle branching (mean of 5 measurements taken from Fig. S4*A*) and a 1.5° x-axis rotation giving the slight concave upper curvature. 2nd order branches were then rotated 90° around the x-axis and 45° around the y-axis and ≥3rd order branches given 340° x-axis and 20° y-axis rotations (Fig. S4*C*). The relatively large number of branches (up to 20 have been observed (21)), relatively even branch spacing and elongate morphology (width usually 20% to 33% of height (21)) were modeled using relatively low values for the lateral branching delay and stem elongation rate (Table S1). Several specimens preserve a holdfast (e.g. see (48) Fig. 2*A*, with holdfast width approximately 72% maximum frond width). The holdfast has been described as ellispoidal (48) or globular (8) and is modeled here using a sphere.

Fig. S4. ***Charnia masoni.*** (*A*) Specimen from the Rawnsley Quartzite, Flinders Ranges, South Australia. South Australia Museum specimen number P36574, described by Nedin & Jenkins (44), photograph courtesy of Jim Gehling (South Australia Museum, Adelaide, Australia). Scale bar 1cm. (*B*) L-system model. Frontal view. (*C*) Rotated view.

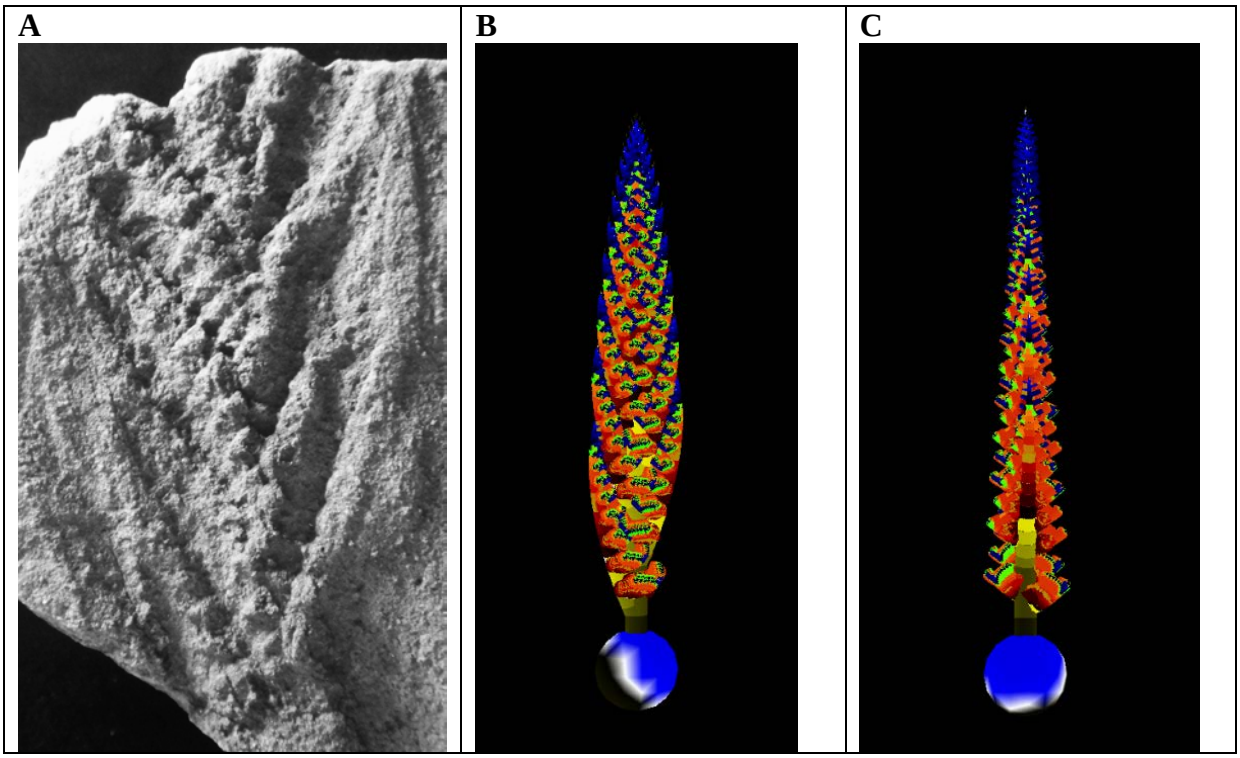

Culmofrons plumosa

This species is morphologically similar to *Beothukis mistakensis*, with an ovate shape (33). However, it is distinguished (33) based on a long basal stem (e.g. with basal stem height 23% of branching frond height in the holotype shown in Fig. S5*A*), slight zig-zag mid-line where the impression of the lateral branches obscures the inferred central stem, and the presence of approximately five alternating primary branches on either side of the central axis. The scalloped outer edge (e.g. visible to the right of Fig. S5*B*) suggests that secondary branches have their emergence points closer to the stem and free apices towards the extremities of the frond (as in *B. mistakensis*). Measurements were used to code y-axis angles for primary branches (y=28°, n=6, Fig. S5*A*). A slight concave upper curvature of the primary branches was modeled using 358° x-axis curvature. Secondary branches were interpreted to have convex upper curvature (of 5°), with a sigmoidal outline (e.g. Fig. *S5B*) visible where secondary branches overlap (33). Secondary branches are only visible on one side of each primary branch. This could suggest that there was only a single row of secondary branches in life (33), which can be modeled using a zero or very low y-axis angle for secondary branching (e.g. see *Trepassia* as modeled below). However, the similar arrangement in *B. mistakenis* has been interpreted as a taphonomic feature, resulting from "folding" (4) or "furling" (45) of secondary branches so that one side of an alternating series is "undisplayed" (45) (as described above) and the model presented here follows this interpretation (Fig. S5*E*). Secondary and tertiary y-axis angles were coded based on measurements from Fig. S5*B* (2^{nd} order, mean=47°, n=8; 3^{rd} order, mean=65°, n=6). Figured specimens of *C. plumosa* are only moderately well preserved in comparison with the best preserved specimen of *B. mistakenis* (Fig. S2*A*; Narbonne et al. (4) Fig. 5.1). However, differences in the strength of the impression of branches on the left and right of the stem (e.g. Fig. S5*B*,*D*) are compatible with a small amount of helical torsion in *C. plumosa* (Fig. S5*D-E*), as reported for *B. mistakensis* (4). The width of the branching frond was measured at 42% of frond height, basal stem height was 23% of branching frond height, and holdfast width was 32% of frond width (holotype, Fig. S5*A*). As some three-dimensionality of the holdfast is preserved (e.g. Fig. S5*C*), this was modeled as a sphere. The long basal stem was modeled using relatively high elongation rate for the basal stem segment (Table S1). The slight zig-zag mid-line visible in the fossil specimens (e.g. Fig. S5*A*) is interpreted to result from the impression of the relatively densely packed alternating primary branches, which slightly overlap the mid-line (Fig. S5*E-G*).

Fig. S5. *Culmofrons plumosa.* (*A*) Image reproduced with permission from Laflamme et al. (33) Fig. 2.2. Holotype specimen. (*B*) Image reproduced with permission from Laflamme et al. (33) Fig. 2.3. (*C*) Image reproduced with permission from Laflamme et al. (33) Fig. 2.7. (*D*) Image reproduced with permission from Laflamme et al. (33) Fig. 2.1. Scale bars 1cm. (*E*) L-system model. Frontal view. (*F*) Rotated view. (*G*) Apical view.

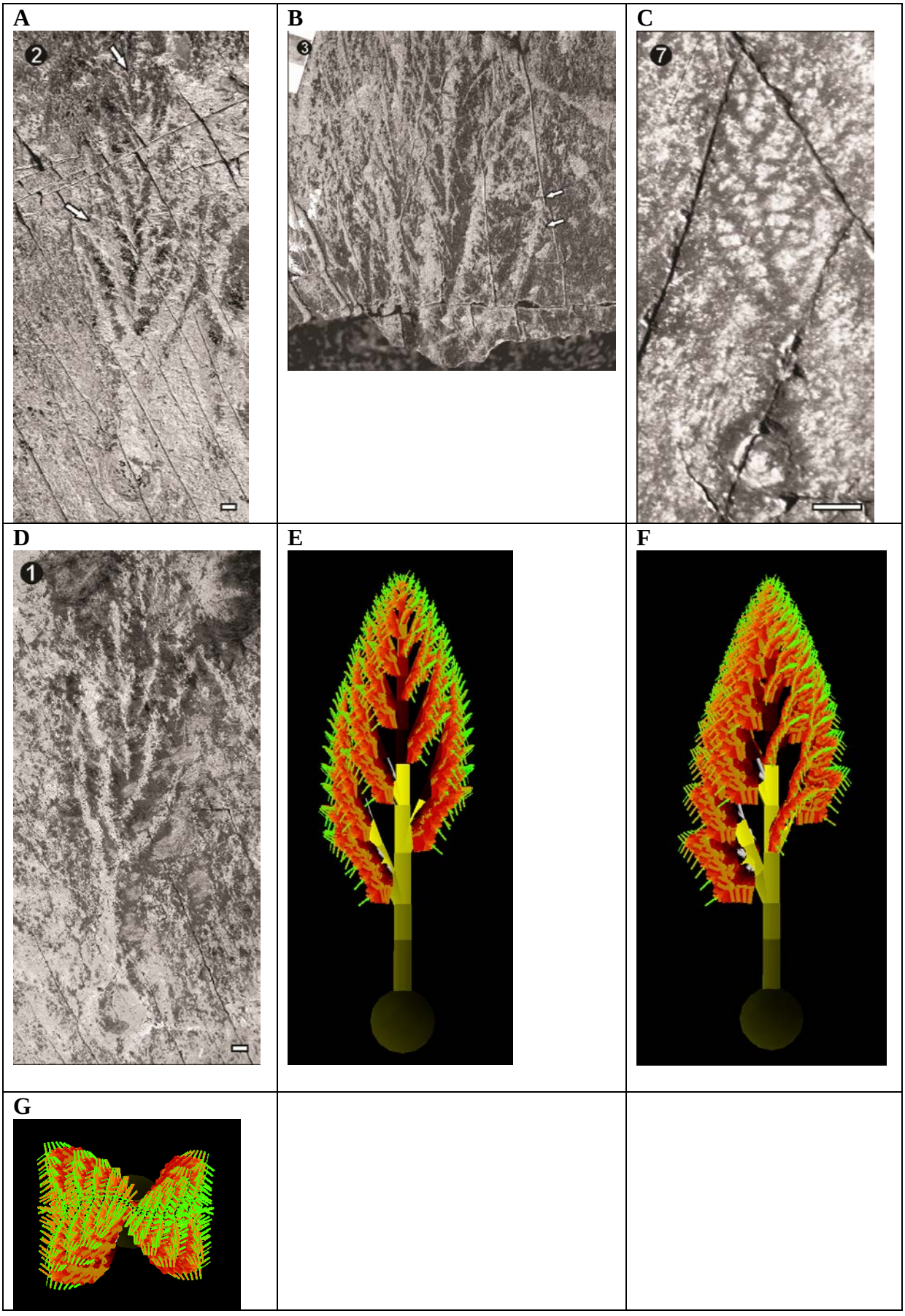
A
B
C
D
E
F
G

Fractofusus andersoni and Fractofusus misrai

Genus *Fractofusus* contains two species: *Fractofusus andersoni* (details here) and *Fractofusus misrai* (details below), represented in Newfoundland by hundreds to thousands of specimens (15). The species share a similar fusisform ("spindle") morphology, which has been interpreted to result from two main poles of growth, one at either end of the central axis (7). Within the L-system formalism used here, this morphology is modeled using a duplication and 180° y-axis rotation of the branching axiom, so that growth proceeds in parallel from two 0-order apices, representing the top and bottom of the stem (as oriented in the images below). The fossils preserve an external mold of the lower surface of the organism, inferred to have been in contact with the sediment in life due to the unusually good preservation of many specimens and the lack of a visible holdfast (15). Three-dimensional curvature of these impressions indicates that each primary branch and its associated higher order branches had a convex outer curvature, modeled here using x-axis curvature of branches of order ≥1 (Table S1). Interestingly, folded specimens of *F. misrai* (see Fig. S7*A*) indicate a similar convex outer curvature for both the upper and lower sides of the organism (15). This morphology is modeled here using rotations of growth axes for the primary branches (90° z-axis rotation around the stem plus primary branch rotations of 90° around the x-axis, 90° around the y-axis and 270° around the z-axis). This gives convex outer curvature to the primary branches on both upper and lower surfaces (as oriented in Fig. S6*C* and Fig. S7*C*) and orients the primary branches perpendicular to the long axis (90°, mean of 13 measurements taken from Gehling & Narbonne (15) Fig.8*C*). Y-axis branching angles for branches of order ≥2 were modeled at 24° for *F. misrai* (mean of 8 secondary branching angle measurements from (15) Fig.8*C*) and 38° for *F. andersoni* (mean of 14 secondary branching angle measurements from (15) Fig.12*C*).

The two *Fractofusus* species are distinguished by the greater number of visible primary branches and more elongate morphology of *F. misrai* (with approximately 20 primary branches and width around 30% of length) compared with *F. andersoni* (with approximately 10 primary branches and width around 65% of length) (15).

Fig. S6. *Fractofusus andersoni.* (*A*) Image reproduced with permission from Gehling & Narbonne (15) Fig.12*C*. Scale bar 1cm. © Canadian Science Publishing or its licensors. (*B*) L-system model. Frontal view. (*C*) Rotated (apical) view.

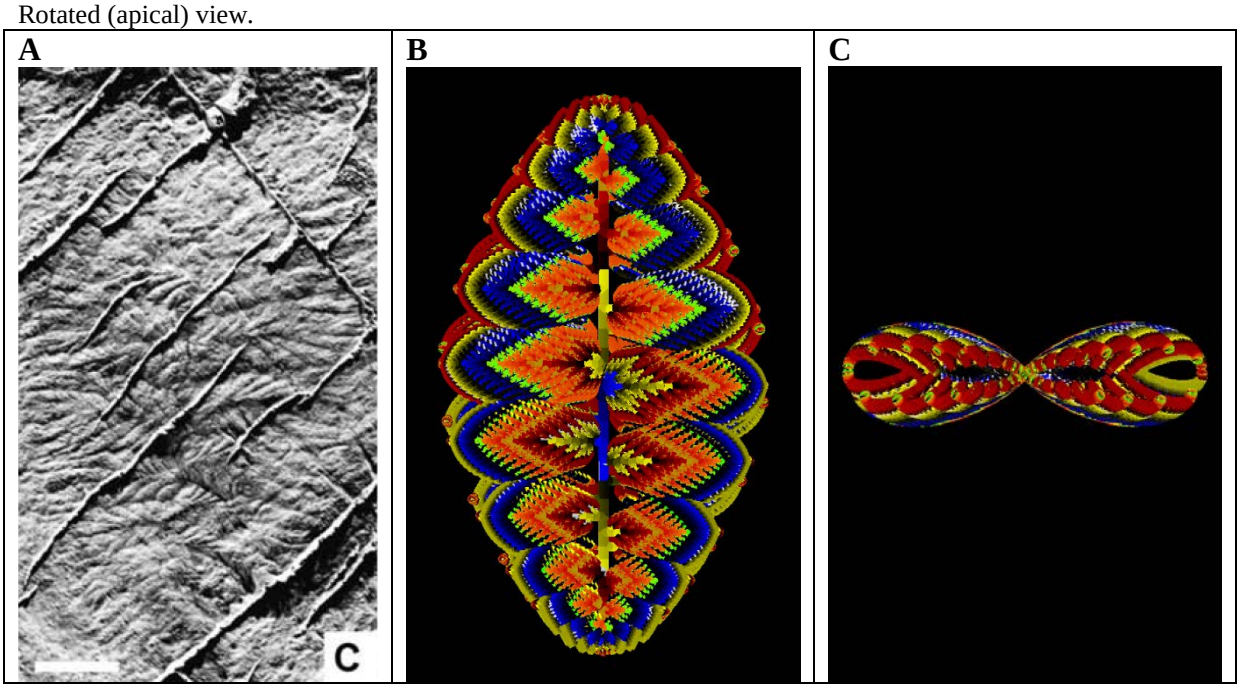

Fig. S7. *Fractofusus misrai.* (*A*) Image reproduced with permission from Gehling & Narbonne (15) Fig.8*C*. Scale bar 1cm. © Canadian Science Publishing or its licensors. (*B*) L-system model. Frontal view. (*C*) Rotated (apical) view.

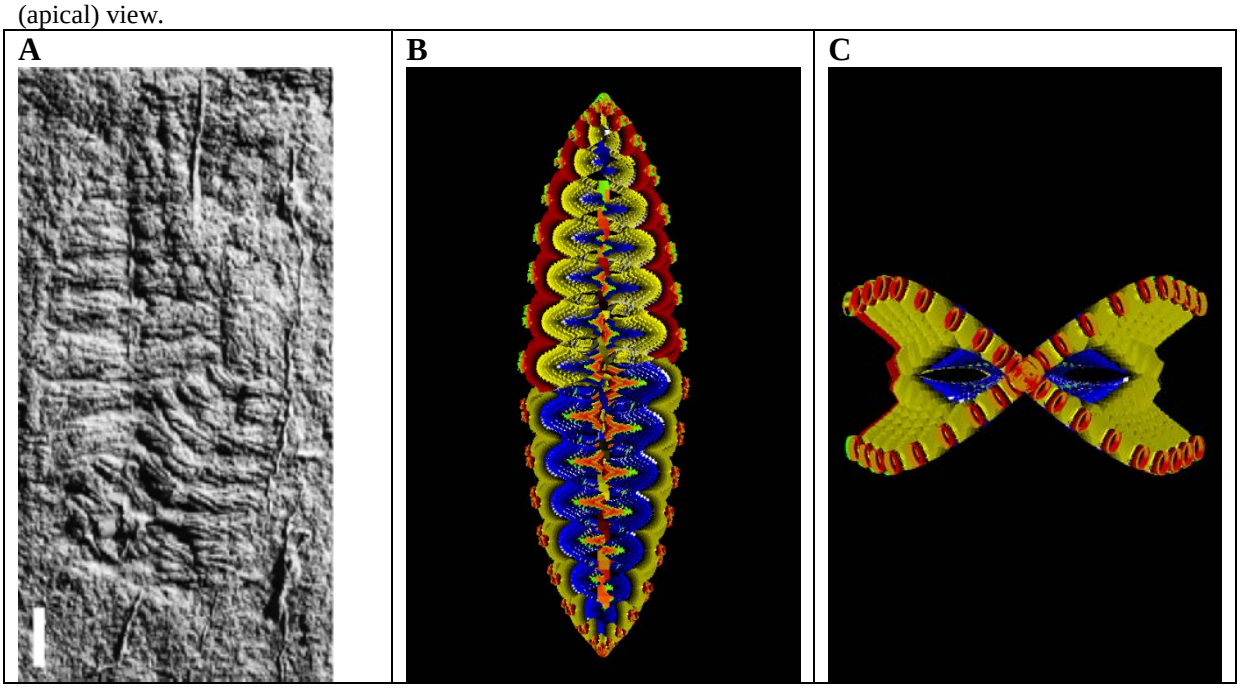

Hapsidophyllas flexibilis

Multiple specimens of this taxon have been reported from Mistaken Point, Newfoundland (49). However, preservation is relatively poor. Large lateral branches appear to emerge from a thick central axis (Fig. S8*A*) and no holdfast is preserved, suggesting that *H. flexibilis* was a benthic recliner, morphologically similar to *Pectinifrons abyssalis* (see model below) (49). Unlike *P. abyssalis*, however, specimens of *H. flexibilis* show impressions of lateral branches on both sides of the inferred central axis (e.g. Fig. S8*B*), although the relative preservation of the two sides varies between specimens (49). The smallest lateral branches lie at either end of the central axis (e.g. Bamforth & Narbonne (49) Fig. 5; Fig. S8*A*), compatible with two main growth axes as suggested for *Fractofusus* (7) and *Pectinifrons* (although lateral branches are of relatively similar lengths throughout). The strength of the impression left by a lateral branch can be seen to decrease progressively towards its apex (Fig. S8*A*) (49), suggesting concave upper curvature of the primary branches (Table S1). In specimen Fig. S8*B* the total height of the organism is approximately 66% of width (as oriented in Fig. S8*B*). These features are here interpreted to indicate a reclining life position, with the central axis in contact with the sediment and two alternating rows of lateral branches curving upwards along their length, into the water column, which were felled to the seabed prior to fossilization (49). Unlike the benthic recliner *Fractofusus* (15), no longitudinally folded specimens have been reported to suggest a double-layered structure. The angle of the large lateral branches (1^{st} order in the L-system numbering used here) from the central axis is variable, and it has been suggested that these were flexible in life (49). The mean of six measurements from the partial specimen shown in Fig. S8*A* was used to code a y-axis branch growth angle of 88°. Eight measurements for the 2^{nd} order branches gave a y-axis mean of 52°.

Fig. S8. *Hapsidophyllas flexibilis.* (*A*) Image reproduced with permission from Bamforth & Narbonne (49) Fig. 5.6. (*B*) Image reproduced with permission from Bamforth & Narbonne (49) Fig. 4.2. Scale bars 1cm increments. (*C*) L-system model. (*D*) Rotated (apical) view.

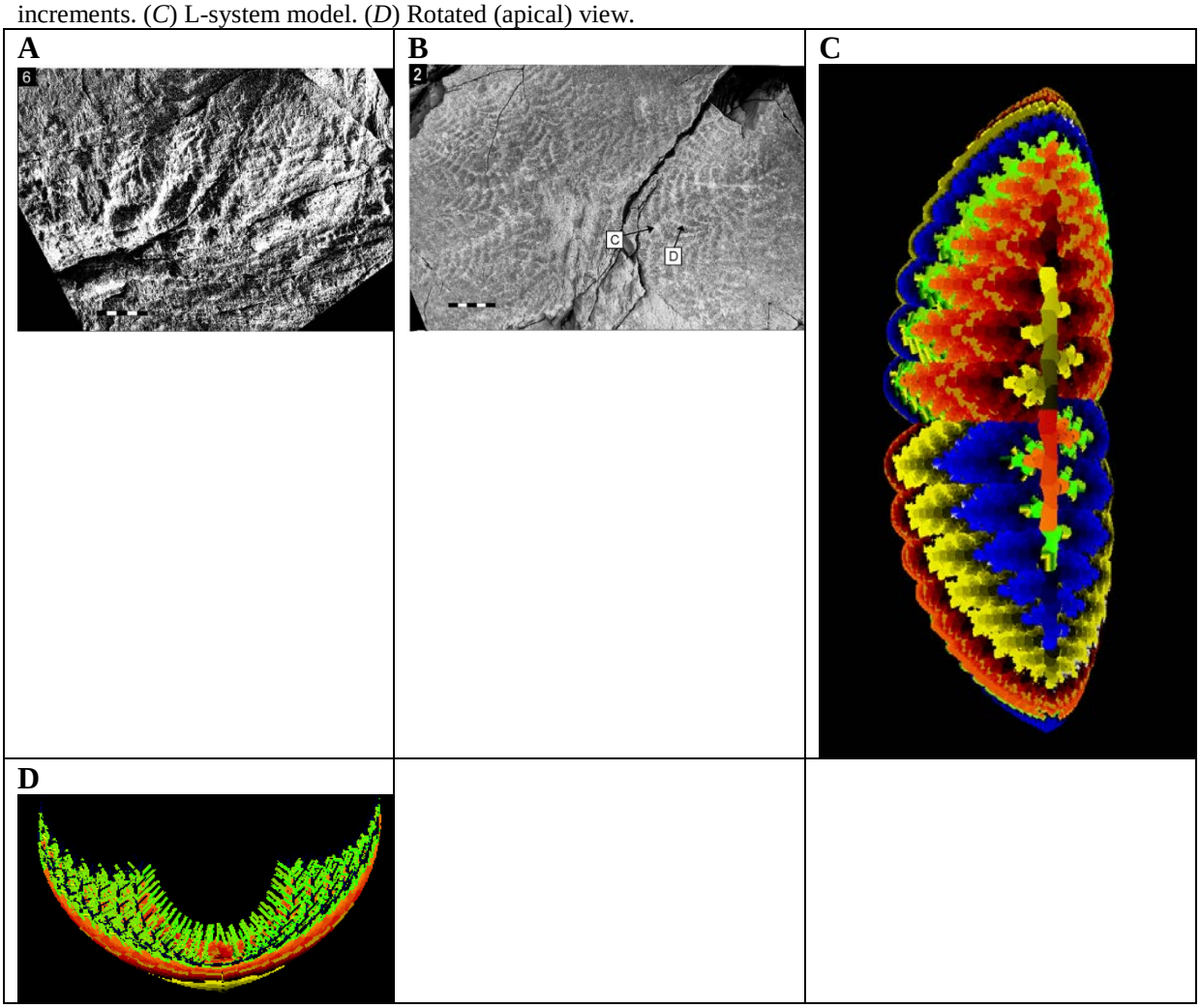

Pectinifrons abyssalis

This species, known from a number of Newfoundland specimens, has a distinctive pectinate (comb-shaped) morphology (Bamforth et al. (50)), with two rows of alternating branches. In the fossil specimens one of these rows overlies the other, so that both are preserved on the same side of the stem (Fig. S9*A*). These primary branches lie approximately perpendicular to the stem in the fossil specimens (50). This morphology was modeled using three rotations for the primary branches (x-axis 90°, y-axis 45°, z-axis 270°). Curvature of the stem is visible in some specimens (e.g. Fig.S9*A*). A C-shaped curve of the stem has been interpreted as a possible biological feature (50). However, fossil specimens show variable stem curvature (e.g. see S-shaped specimen illustrated in (50) Fig. 7). Therefore, this is interpreted here as taphonomic variability and the stem is modeled as uncurved in the life position (Fig. S9*B*). Branching structure for order 2 is poorly preserved however this is visibly acute (and was modeled here using an approximate y-axis branching angle of 38°).

Fig. S9. ***Pectinifrons abyssalis.*** (*A*) Image reproduced with permission from Bamforth et al. (50) Fig. 4.1. Scale bar 1cm increments. (*B*) L-system model. Frontal view. (*C*) Rotated (apical) view.

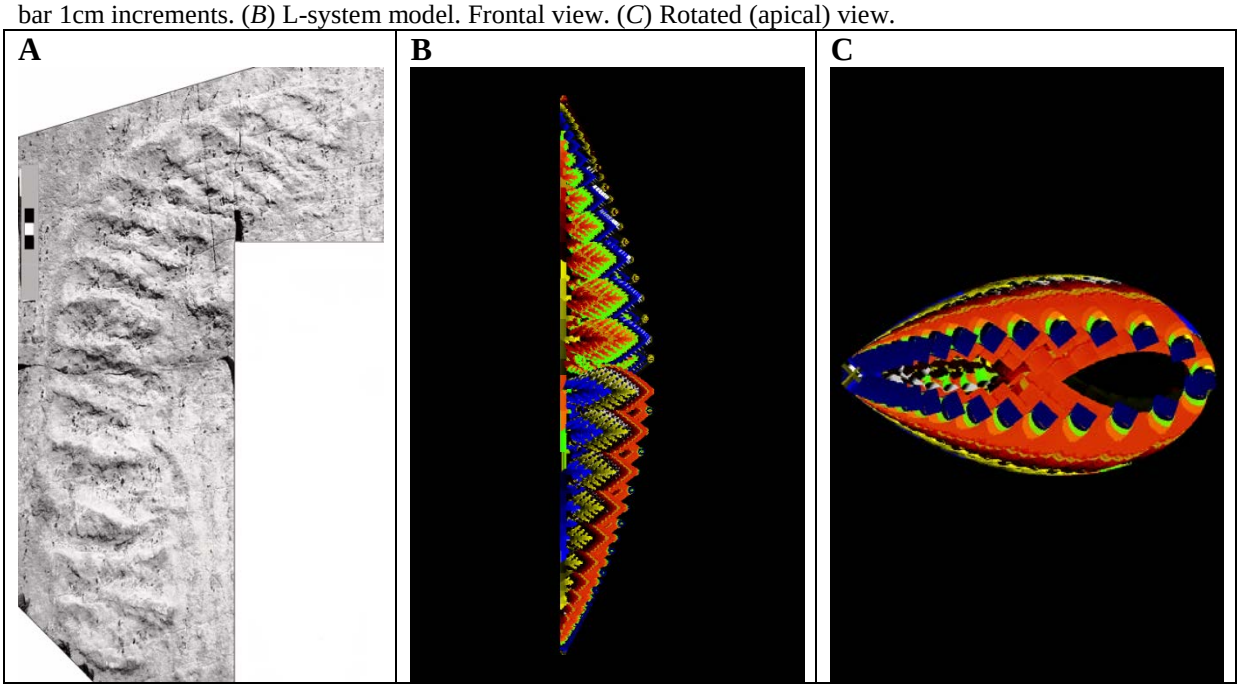

Rangea schneiderhoehni

In this species, the alternating branches are thought to be arranged into >2 vanes or rows (51). Interpretations of the number of vanes differ, at three (51), four (52) and five to six (35). Here, the multi-vane arrangement is interpreted to result from a low y-axis angle of 8° for primary branching, combined with z-axis rotations (of 202.5° and 135°, respectively, for the primary and secondary branches). These rotations orient the secondary branches into four vertical rows, compatible with previous suggestions of four “vanes” (Fig. S10*G*), which form a tetraradial arrangement when viewed from above (52). In long-axis rotations (e.g. Fig. S10*C*), only three of these rows are clearly visible. This arrangement is compatible with previous observations of up to three vanes in flattened fossil specimens (e.g. Fig. S10*A*), where a third vane may be visible when only partially overlapped by the vane above it (51). New specimens confirm the presence of a central stem (“axial stalk”) and “axial bulb” (35), interpreted here as a small holdfast. Holdfast width was estimated at approximately 18% of maximum frond width from Vickers-Rich et al. (35) Fig. 6.1. Vickers-Rich et al. (35) suggested that new three-dimensional specimens from southern Namibia preserve five to six

vanes. However, the model presented here is similar in basal view to their figured specimen (compare Fig. S10*E*-*F*). The grouping of secondary and higher branches on primary branches that lie very close to the stem is consistent with partial specimens that reveal branch positions (compare partial fossil specimen Fig. S10*H* and a partial model in which only the basal primary branches are displayed Fig. S10*I*). The relatively compact body form was modeled using low to moderate values for lateral branching delays and elongation rates (Table S1).

Fig. S10. ***Rangea schneiderhoehni.*** (*A*) Specimen from the Kliphoek Member, Dabis Formation, Namibia. Image reproduced with permission from Grazhdankin & Seilacher (51) Fig. 2. Scale bar 1cm. (*B*) L-system model. Frontal view. (*C*) Rotated view. (*D*) Image reproduced with permission from Vickers Rich et al. (35) Fig. 8.1. Specimen NESM F635-c lower view. (*E*) Image reproduced with permission from Vickers Rich et al. (35) Fig. 8.2. Specimen NESM F635-c upper view. Scale bars 1cm. (*F*) L-system model. View from below. (*G*) View from above. (*H*) Partial specimen. Image reproduced with permission from Grazhdankin & Seilacher (51) Fig.7. Scale bar 1cm. (*I*) Partial model illustrating the relative positions of two sequential lateral branches.

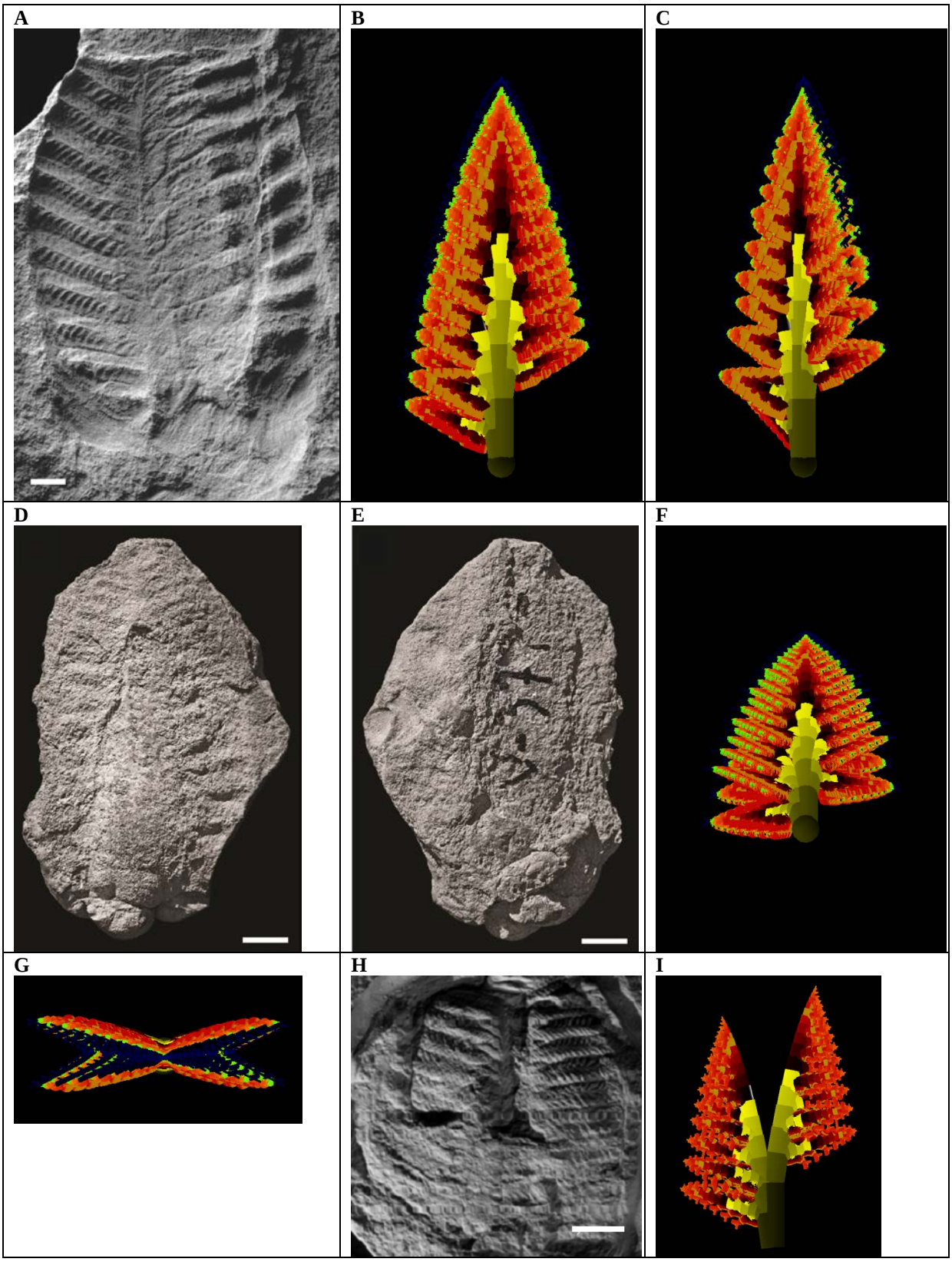
A
B
C
D
E
F
G
H
I

Trepassia wardae

Initially described as *Charnia wardi* (1) and redefined as *Trepassia wardae* (4), this is an elongate species, with a width to height ratio of 1.6:6 cm (width 26% height) measured from an exceptionally preserved 3-D specimen from Spaniard's Bay (4). Specimens from the Drook Formation, preserved as flattened impressions, are the longest known Ediacaran fronds, up to 1.85 m in height (with width <10% of height (1)). Previous interpretations have suggested that the primary and secondary branches originate close to the main stem, to which they may both have been attached (4). As a result, most primary and secondary branch origins are concealed. However, a measurement for the lowest primary branch, visible in Narbonne et al. (4) Fig. 10.4 (Fig. S11*D*) gave a y-axis branching angle of 4°. An x-axis curvature of 7° for the 2nd order branches was used to model their convex upper curvature. Here, primary and secondary branches are interpreted to emerge at an acute angle so that both lie close to the main body axis. The branches acute to perpendicular to the stem (mean=82°, n=6) are then interpreted to be 3rd order (rather than 2nd order as previously suggested by Narbonne et al. (4)). This branching pattern is compatible with both details of fossil morphology (compare details Fig. S11*D* and Fig. S11*E* below) and the elongate overall morphology of the frond, which is increased by the near-vertical orientation of the 1st and 2nd order branches. Only one side of the 1st and 2nd order branches is visible in front or back view (4). This is interpreted as the result of a z-axis rotation of 90° for the 1st order branches. This model used a moderate lateral branching delay and a moderate increase in elongation rate relative to the stem for branches of order ≥2 (Table S1). Holdfast width was estimated at approximately 47% of frond width, from Narbonne et al. (4) Fig. 10.4.

Fig. S11. ***Trepassia wardae.*** (*A*) Specimen from Spaniard's Bay, Newfoundland. Image reproduced with permission from Narbonne et al. (4) Fig. 10.1. Scale bar 1cm. (*B*) L-system model. Frontal view. (*C*) Rotated view. (*D*) Detail of Narbonne et al. (4) Fig. 10.4. Scale bar 1cm. (*E*) Detail from L-system model.

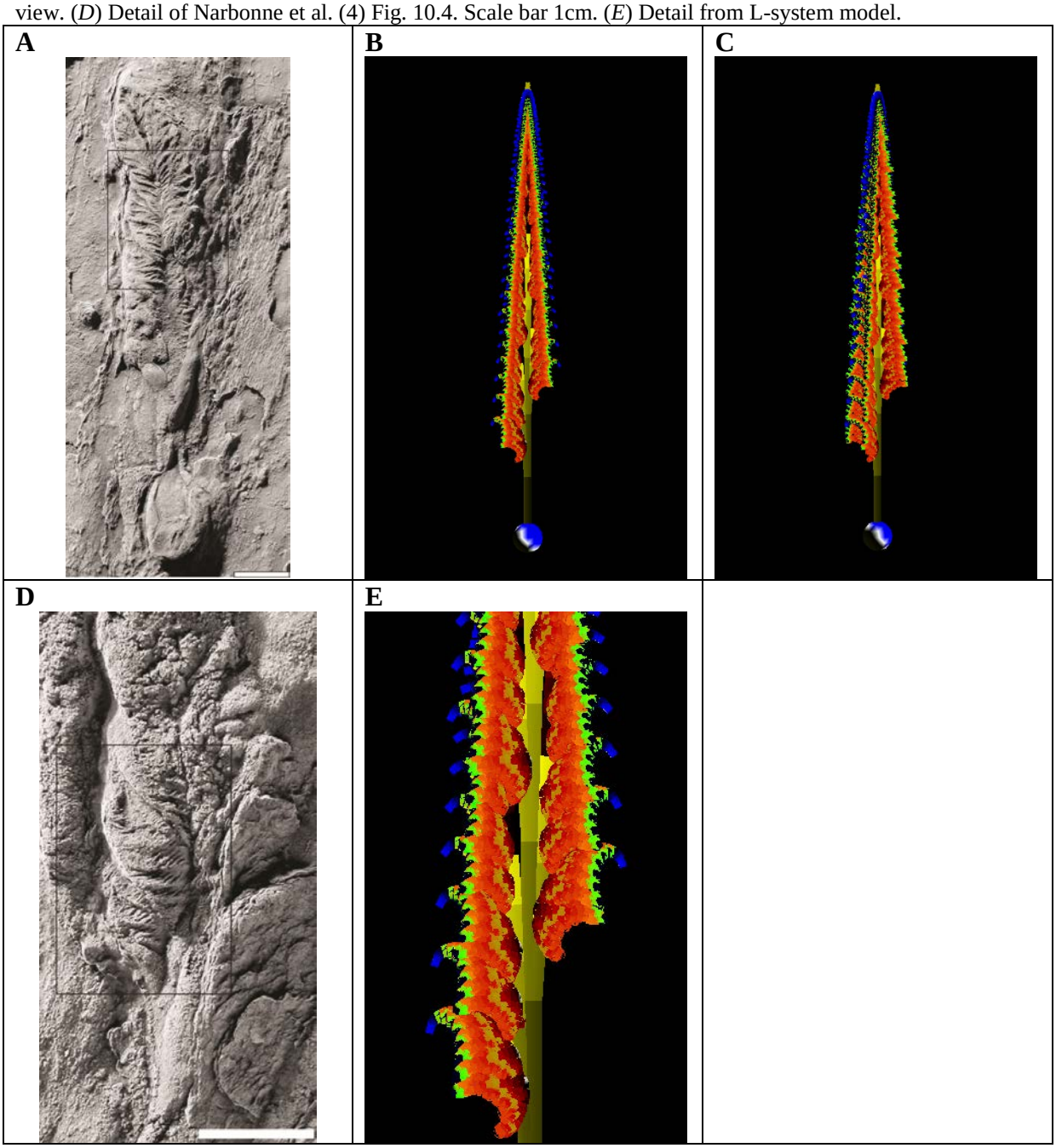

Fig. S12. Dendrogram showing hierarchical clustering of modeled rangeomorph dimensions (see Table S2 for values). Species labels: 1. *Avalofractus abaculus* 2. *Beothukis mistakensis* 3. *Bradgatia linfordensis* 4. *Charnia masoni* 5. *Culmofrons plumosa* 6. *Fractofusus andersoni* 7. *Fractofusus misrai* 8. *Hapsidophyllas flexibilis* 9. *Pectinifrons abyssalis* 10. *Rangea schneiderhoehni* 11. *Trepassia wardae*.

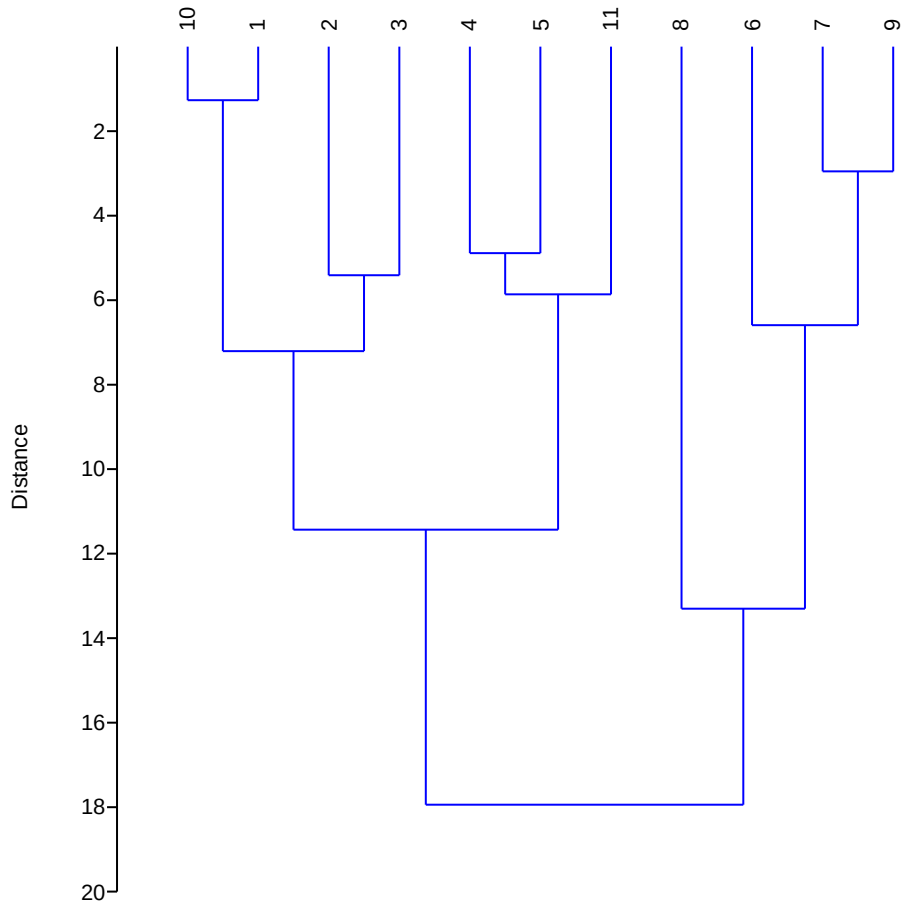

Fig. S13. Fractal dimensions. Box counting estimates of the fractal dimension in 2D and 3D. Input images are linear "skeletons" of the modeled branching structure.

A 2D projection *A. abaculus* model

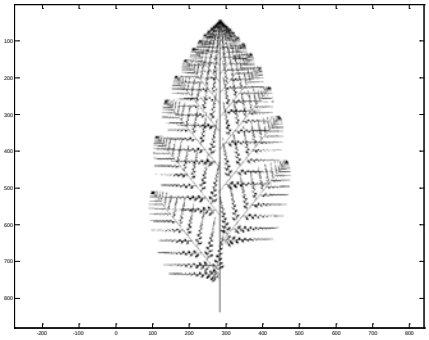

B 2D box counting dimension

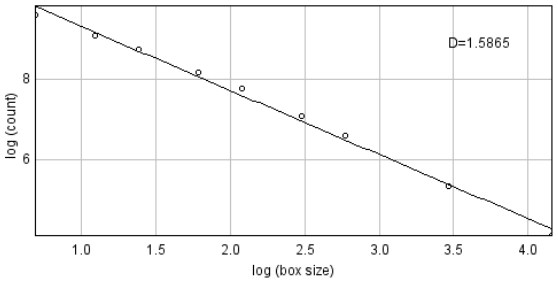

C 3D model *A. abaculus*

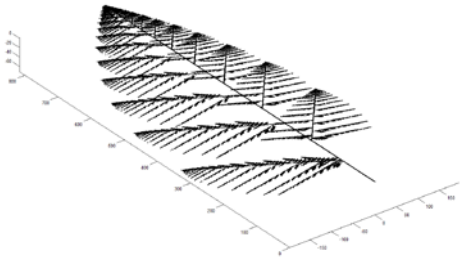

D 3D box counting dimension

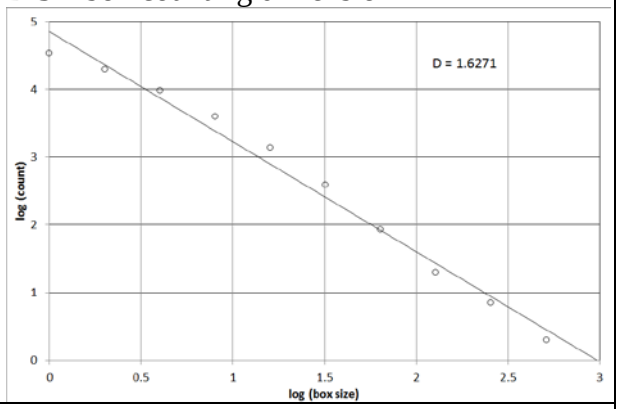

E 2D projection *B. mistakensis* model

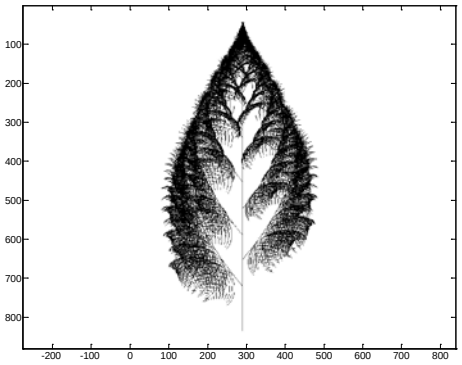

F 2D box counting dimension

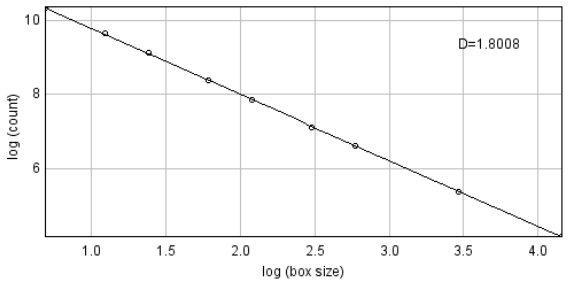

G 3D model *B. mistakensis*

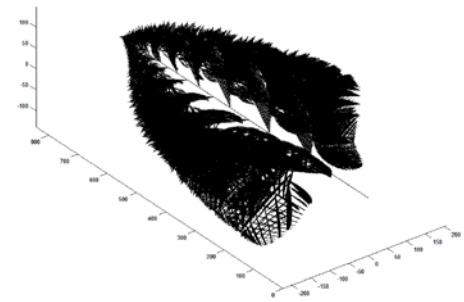

H 3D box counting dimension

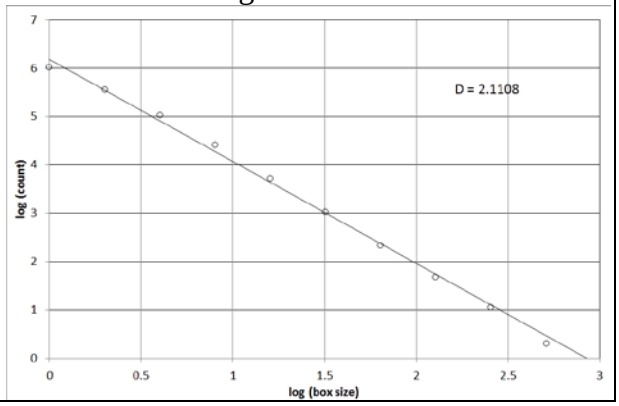

I 2D projection *B. linfordensis* model

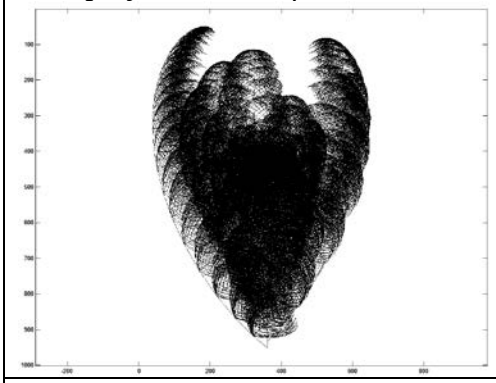

J 2D box counting dimension

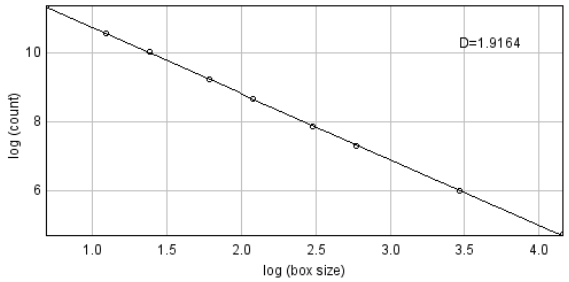

K 3D model *B. linfordensis*

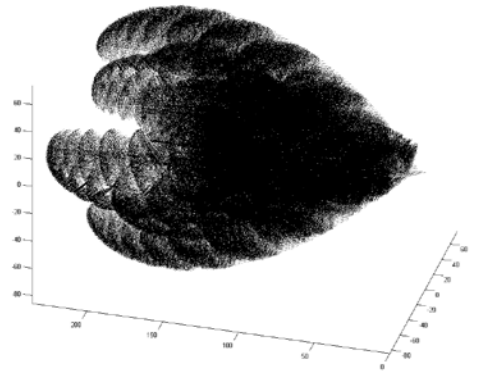

L 3D box counting dimension

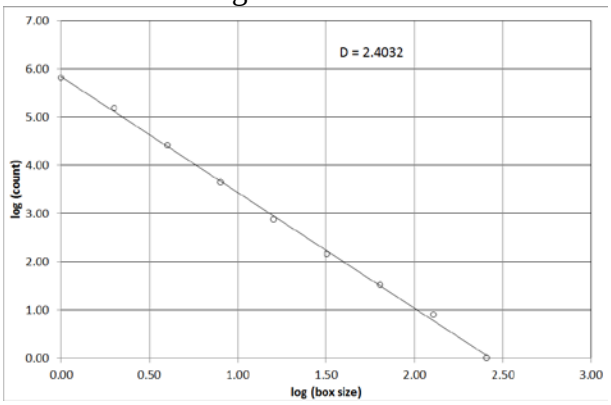

M 2D projection *C. masoni* model

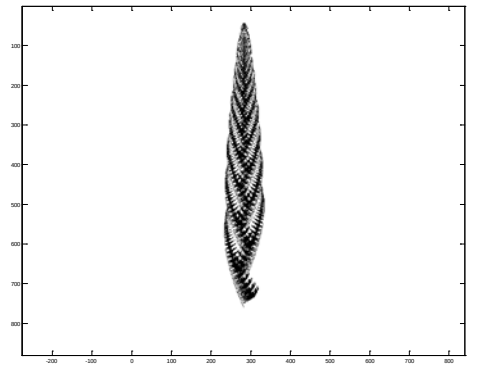

N 2D box counting dimension

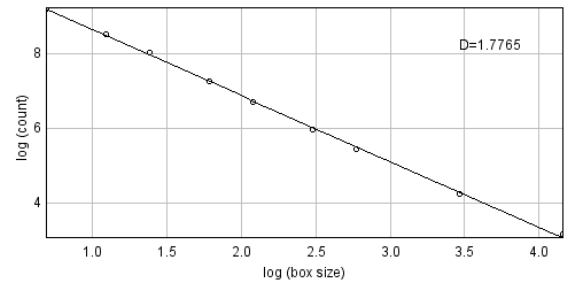

O 3D model *C. masoni*

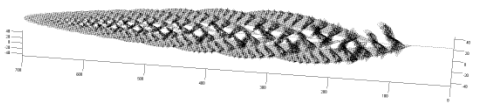

P 3D box counting dimension

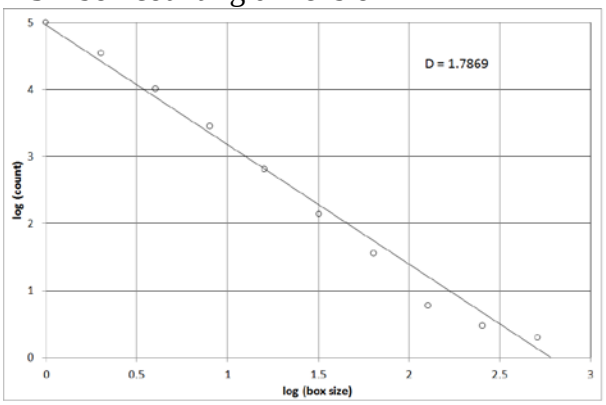

Q 2D projection *C. plumosa* model

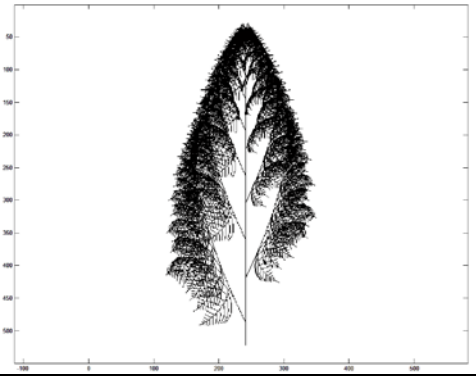

R 2D box counting dimension

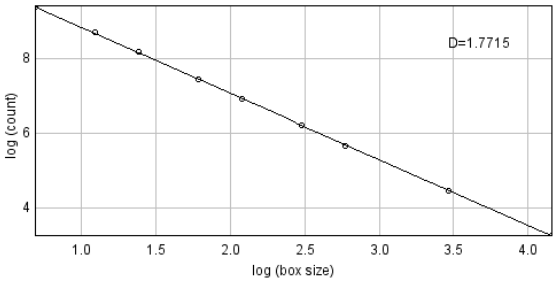

S 3D model *C. plumosa*

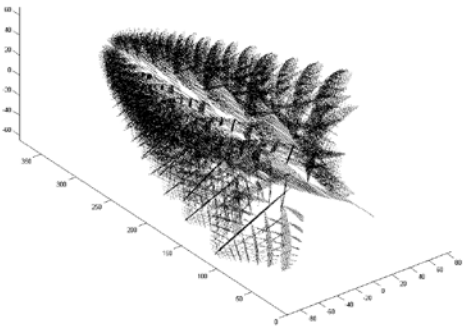

T 3D box counting dimension

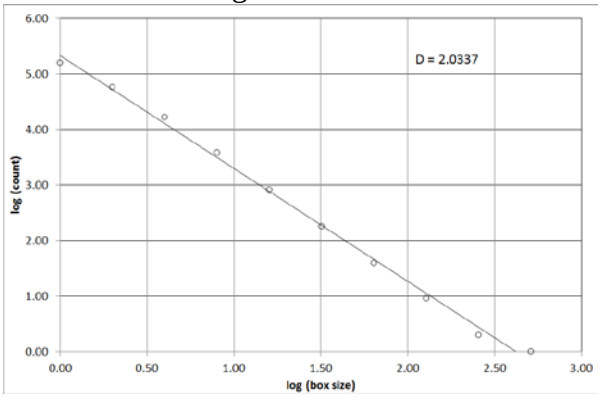

U 2D projection *F. andersoni* model

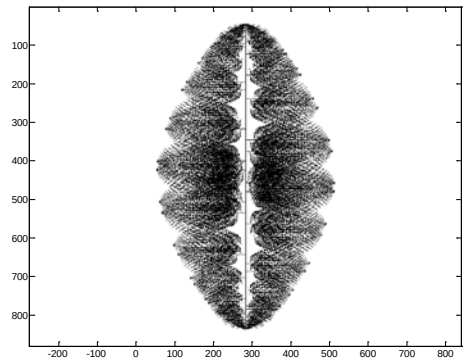

V 2D box counting dimension

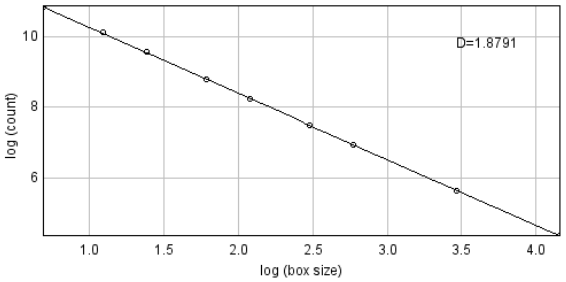

W 3D model *F. andersoni*

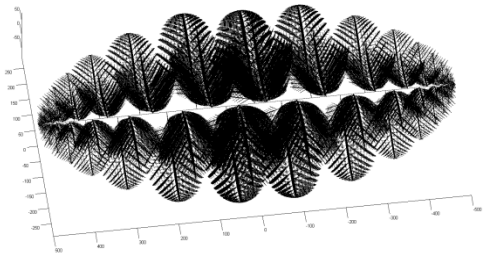

X 3D box counting dimension

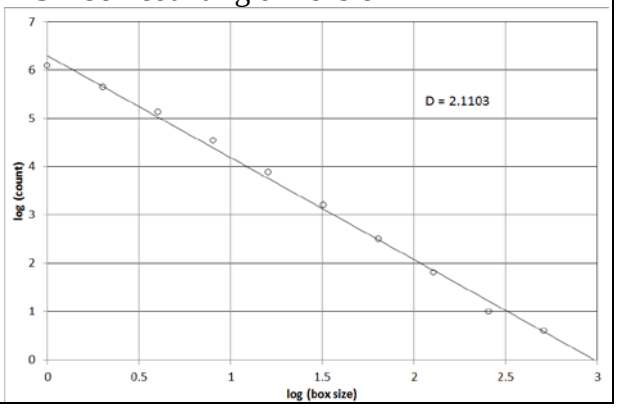

Y 2D projection *F. misrai* model

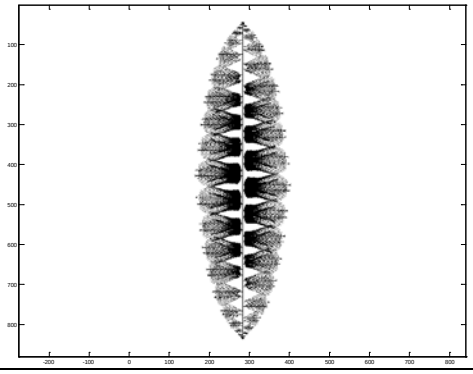

Z 2D box counting dimension

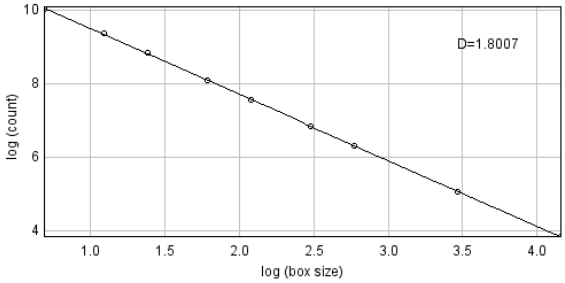

AA 2D projection *H. flexibilis* model

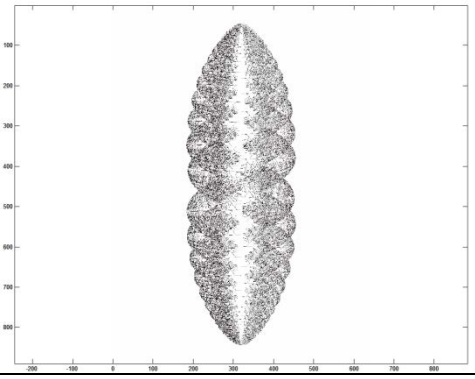

AB 2D box counting dimension

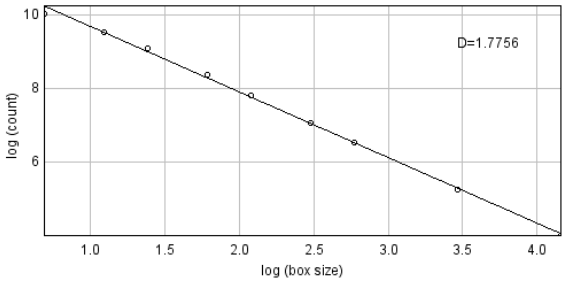

AC 3D model *H. flexibilis*

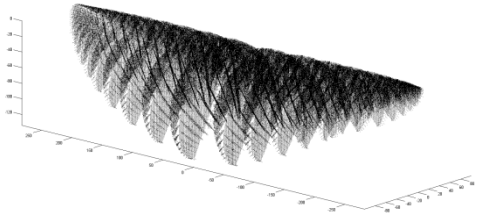

AD 3D box counting dimension

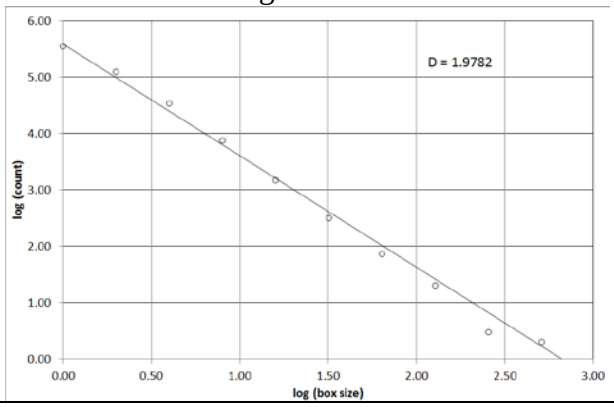

AE 2D projection *P. abyssalis* model

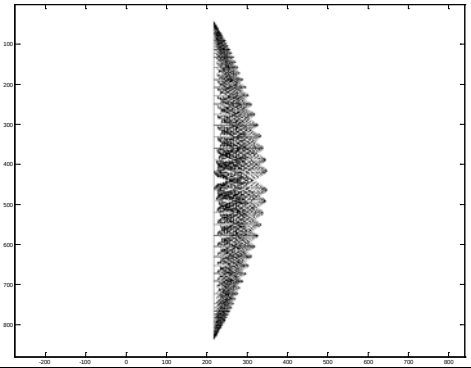

AF 2D box counting dimension

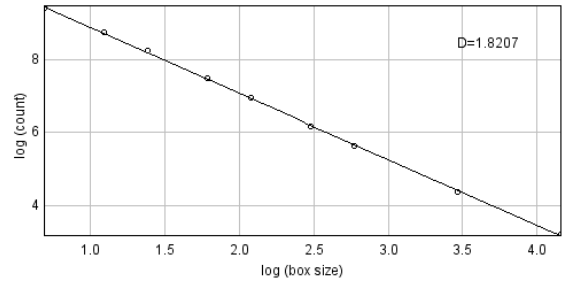

AG 2D projection *R. schneiderhoehni* model

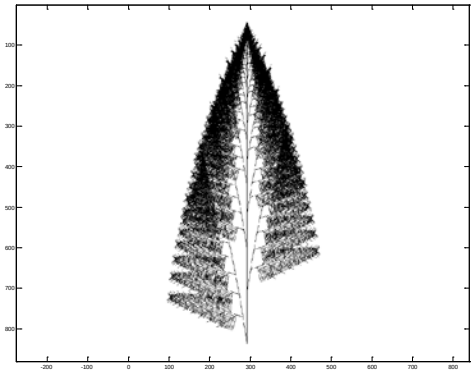

AH 2D box counting dimension

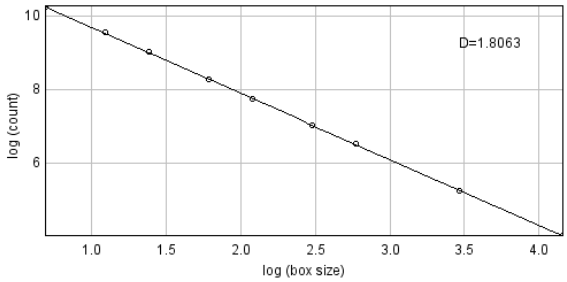

AI 3D model *R. schneiderhoehni*

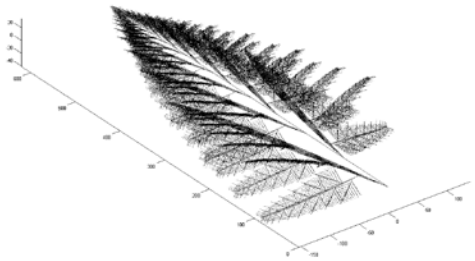

AJ 3D box counting dimension

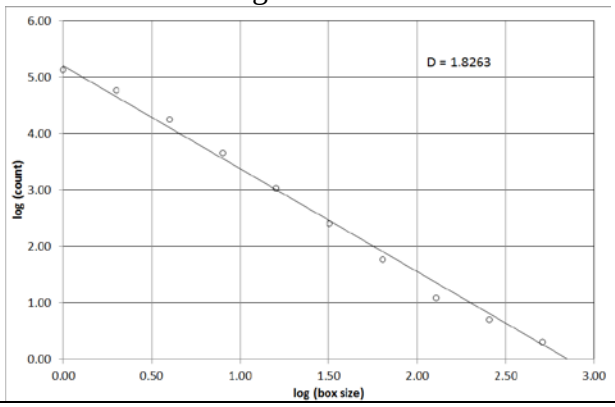

AK 2D projection *T. wardae* model

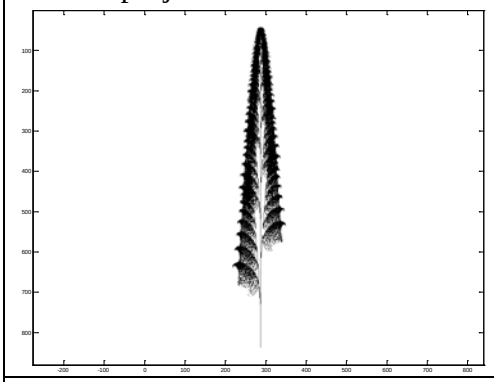

AL 2D box counting dimension

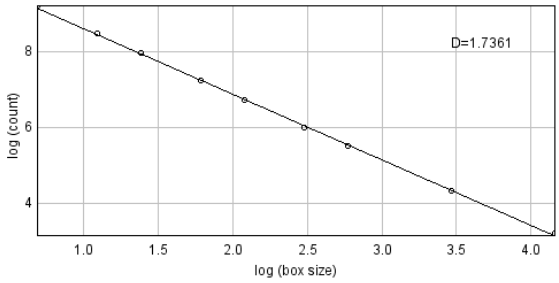

AM 3D model *T. wardae*

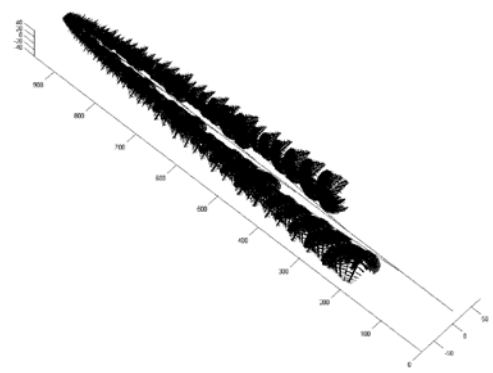

AN 3D box counting dimension

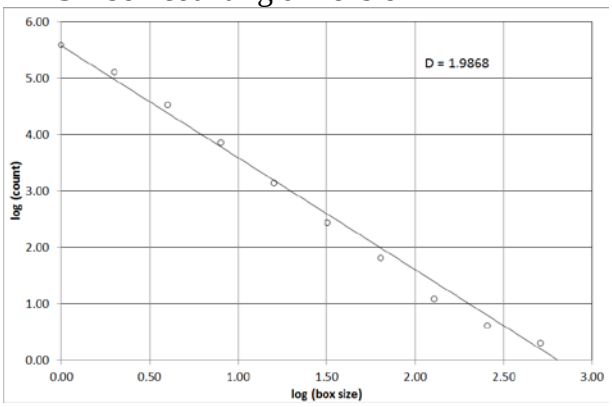

Table S1. L-system parameters

Species	Parameter Branch order	Holdfast diameter (L-system world units)	Elongation rate 0	 1	 2	 ≥3
Avalofractus abaculus		60	1.115	1.125	1.125	1.125
Beothukis mistakensis		80	1.115	1.120	1.130	1.130
Bradgatia linfordensis		5	1.06	1.114	1.07	1.07
Charnia masoni		50	1.100	1.085	1.050	1.050
Culmofrons plumosa		30	1.115	1.114	1.13	1.13
Fractofusus andersoni		N	1.100	1.100	1.125	1.125
Fractofusus misrai		N	1.110	1.080	1.120	1.120
Hapsidophyllas flexibilis		N	1.1	1.1	1.11	1.1
Pectinifrons abyssalis		N	1.115	1.125	1.125	1.125
Rangea schneiderhoehni		20	1.115	1.110	1.110	1.050
Trepassia wardae		30	1.115	1.115	1.130	1.130

Elongation rate Basal stem segment	Branching delay (prop. iterations) 0	 1	 2	 ≥3	x curvature angle (°) 0	y zig-zag angle (°) 0
1.125	0.00	0.21	0.21	0.24	0.0	0.0
1.040	0.00	0.24	0.16	0.16	0.0	0.0
N	0.00	0.21	0.08	0.08	0.0	0.0
N	0.00	0.13	0.18	0.21	0.0	0.0
1.1	0.00	0.29	0.21	0.16	0.0	0.0
N	0.00	0.16	0.24	0.24	0.0	0.0
N	0.00	0.00	0.22	0.11	0.0	0.0
N	0.00	0.00	0.26	0.29	0.0	0.0
N	0.00	0.20	0.20	0.23	0.0	0.0
N	0.00	0.24	0.16	0.18	0.0	0.0
N	0.00	0.24	0.16	0.16	0.0	0.0

z torsion angle (°) 0	x curvature angle (°) 1	y zig-zag angle (°) 1	z rotation angle (°) 1	x curvature angle (°) ≥2
0.0	0.0	0.0	0.0	0.0
355.0	357.0	0.0	0.0	5.0
42.5	355.0	0.0	0.0	355.0
0.0	1.5	0.0	0.0	359.5
357.0	358.0	0.0	0.0	5.0
90.0	4.0	0.0	0.0	4.0
90.0	1.0	0.0	0.0	2.0
0.0	5.0	0.0	0.0	5.0
0.0	4.0	0.0	0.0	4.0
0.0	358.0	0.0	135.0	359.0
0.0	0.0	0.0	0.0	7.0

y zig-zag angle (°) ≥2	z rotation angle (°) ≥2	x branching angle (°) 1	y branching angle (°) 1	z branching angle (°) 1
0.0	0.0	15.0	38.0	0.0
0.0	0.0	0.0	43.0	90.0
0.0	0.0	0.0	55.0	90.0
0.0	0.0	0.0	26.0	270.0
0.0	0.0	0.0	28.0	90.0
0.0	0.0	90.0	90.0	270.0
0.0	0.0	90.0	90.0	270.0
0.0	0.0	0.0	88.0	0.0
0.0	0.0	90.0	45.0	270.0
0.0	0.0	0.0	8.0	202.5
0.0	0.0	0.0	4.0	90.0

x branching angle (°) 2	y branching angle (°) 2	z branching angle (°) 2	x branching angle (°) ≥3
15.0	47.0	0.0	15.0
0.0	46.0	0.0	0.0
0.0	45.0	0.0	355.0
90.0	45.0	0.0	340.0
0.0	47.0	0.0	0.0
0.0	38.0	0.0	0.0
0.0	24.0	0.0	0.0
0.0	52.0	0.0	0.0
0.0	38.0	0.0	0.0
0.0	64.0	345.0	0.0
0.0	0.0	0.0	0.0

y branching angle (°) ≥3	z branching angle (°) ≥3
47.0	0.0
56.0	0.0
0.0	0.0
20.0	0.0
65.0	0.0
38.0	0.0
24.0	0.0
52.0	0.0
38.0	0.0
45.0	0.0
82.0	0.0

Table S2. Estimated functional properties

Species	Length fossil (cm)	Source of length estimate	Estimated width (cm)
Avalofractus abaculus	9.4	Holotype measurement from Narbonne et al 2009	3.2
Beothukis mistakensis	14.0	Mean from Brasier and Antcliffe 2009	5.7
Bradgatia linfordensis	12.2	Mean from Flude & Narbonne 2008	8.1
Charnia masoni	20.0	Upper limit in classification of Laflamme et al 2007	2.7
Culmofrons plumosa	20.3	Mean from Laflamme et al 2012	7.0
Fractofusus andersoni	7.3	Range median from Gehling & Narbonne 2007	7.3
Fractofusus misrai	12.5	Range median from Gehling & Narbonne 2007	12.5
Hapsidophyllas flexibilis	23.2	Mean from Bamforth & Narbonne 2009	23.2
Pectinifrons abyssalis	15.0	Mean from Bamforth et al 2008	15.0
Rangea schneiderhoehni	9.0	Estimate from Fig 8 of Vickers-Rich et al 2013	4.4
Trepassia wardae	25.0	Mean from Laflamme et al 2007 and Narbonne et al 2009	3.6
mean	15.3		8.4
variance	36.2		38.9

			Tissue thickness (mm)	0
Estimated height (cm)	**Estimated depth (cm)**	**Bounding volume (cm^3)**	**Relative bounding volume (longest axis scaled to 1)**	**Total SA (cm^2)**
9.4	1.1	34.0	0.04	77.1
14.0	3.5	279.0	0.10	455.6
12.2	8.0	796.8	0.44	1591.0
20.0	2.7	143.2	0.02	1067.7
20.3	5.0	712.8	0.09	1332.3
1.1	4.2	33.7	0.09	486.6
1.9	3.8	89.5	0.05	1599.8
5.5	8.1	1037.3	0.08	5787.8
1.2	2.4	42.4	0.01	221.1
9.0	1.1	42.9	0.06	218.0
25.0	1.9	175.8	0.01	1159.6
10.9	3.8	307.9	0.09	1272.4
68.7	6.0	131910.1	0.01	2558640.6

0.1	0.5	1	0.1	0.5	1
Tissue volume (cm^3)	**Tissue volume (cm^3)**	**Tissue volume (cm^3)**	**SA/V (cm^2/cm^3)**	**SA/V (cm^2/cm^3)**	**SA/V (cm^2/cm^3)**
0.8	5.8	15.6	92.1	13.3	4.9
1.3	7.0	15.3	352.4	65.2	29.8
12.5	94.2	289.4	127.0	16.9	5.5
11.0	64.3	152.5	97.5	16.6	7.0
10.1	63.5	165.6	132.0	21.0	8.0
6.4	51.7	152.9	76.5	9.4	3.2
15.7	106.4	282.9	102.0	15.0	5.7
43.1	271.2	706.7	134.4	21.3	8.2
1.2	7.6	19.2	182.8	29.0	11.5
2.5	16.1	41.0	86.4	13.5	5.3
5.8	31.3	68.5	200.0	37.0	16.9
10.0	65.4	173.6	143.9	23.5	9.6
145.6	5894.7	41293.6	6309.6	252.7	58.9

0	0
Branching frond SA (cm^2)	**Frond plane SA (cm^2)**
73.2	20.5
435.0	68.0
1590.0	71.5
1047.1	37.6
1309.6	80.9
486.6	24.3
1599.8	37.3
5787.8	153.3
221.1	29.7
216.9	37.6
1151.8	85.1
1265.4	58.7
2563957.8	1522.7

Table S3. Fossil ranges

Assemblage	Formation	Country	Age (Ma)	Reference
Nama	Dabis	Namibia	547-541	Vickers-Rich et al 2013
White Sea	Zimnegory	Russia	555.3 ± 0.3	Grazhdankin 2004
White Sea	Verkhovka	Russia	558.3 ± 1	Grazhdankin 2004
Ediacara (White Sea)	Rawnsley Quartzite	Australia	556 ± 24	Geoscience Australia
Charnwood/Mercian (Avalon)	Bradgate - Beacon Hill	UK	563 ± 1.9	Wilby et al 2011
Avalon	Fermeuse	Canada		
Avalon	Trepassey	Canada	565 ± 3	Narbonne et al 2009
Avalon	Mistaken Point	Canada	565 ± 3	Narbonne et al 2009
Avalon	Briscal	Canada		
Avalon	Drook	Canada	575	Narbonne et al 2009

Avalofractus abaculus	Reference	***Beothukis mistakensis***	Reference	***Bradgatia linfordensis***
		present	Narbonne et al 2009	present
				present
		present	Narbonne et al 2009	
present	Narbonne et al 2009	present	Narbonne et al 2009	present
		present	Brasier & Antcliffe 2009	present
		present	Narbonne et al 2009	present

Reference	***Charnia masoni***	Reference	***Culmofrons plumosa***	Reference
	present	Narbonne & Gehling 2003		
Gehling & Droser 2013	present	Nedin & Jenkins 1998		
Flude & Narbonne 2008	present	Wilby et al 2011		
Flude & Narbonne 2008	present	Narbonne et al 2009		
Flude & Narbonne 2008	present	Narbonne et al 2009	present	Laflamme et al 2012
Flude & Narbonne 2008	present	Narbonne et al 2009	present	Laflamme et al 2012
	present	Liu et al 2012		

Fractofusus andersoni	Reference	***Fractofusus misrai***	Reference	***Hapsidophyllas flexibilis***
present	Gehling & Narbonne 2007			
present	Gehling & Narbonne 2007	present	Gehling & Narbonne 2007	present
present	Gehling & Narbonne 2007			

Reference	***Pectinifrons abyssalis***	Reference	***Rangea schneiderhoehni***
			present
			present
			present
	present	Bamforth et al 2008	
Bamforth & Narbonne 2009	present	Bamforth et al 2008	

Reference	***Trepassia wardae***	Reference
Grazhdankin & Seilacher 2005		
Grazhdankin 2004		
Grazhdankin 2004		
	present	Narbonne et al 2009
	present	Narbonne et al 2009
	present	Narbonne & Gehling 2003

Supporting Video Legends

Video S1. Video animation of the L-system growth model for *Beothukis mistakensis*.

Video S2. Video animation of the L-system growth model for *Charnia masoni*.

Video S3. Video animation of the L-system growth model for *Hapsidophyllas flexibilis*.

Supporting References

45. Brasier MD, Antcliffe JB (2009) Evolutionary relationships within the Avalonian Ediacara biota: new insights from laser analysis. *J Geol Soc London* 166: 363-384.
46. Braybrook SA, Kuhlemeier C (2010) How a plant builds leaves. *The Plant Cell* 22:1006-1018.
47. Grazhdankin D (2004) Patterns of distribution in the Ediacaran biotas: facies versus biogeography and evolution. *Paleobiology* 30:203-221.
48. Wilby PR, Carney JN, Howe MPA (2011) A rich Ediacaran assemblage from eastern Avalonia: evidence of early widespread diversity in the deep ocean. *Geology* 39:655-658.
49. Bamforth EL, Narbonne GM (2009) New Ediacaran rangeomorphs from Mistaken Point, Newfoundland, Canada. *J Paleont* 83:897-913.
50. Bamforth EL, Narbonne GM, Anderson MM (2008) Growth and ecology of a multi-branched Ediacaran rangeomorph from the Mistaken Point assemblage, Newfoundland. *J Paleont* 82:763-777.
51. Grazhdankin D, Seilacher A (2005) A re-examination of the Nama-type Vendian organism *Rangea schneiderhoehni*. *Geol Mag* 142:571-582.
52. Dzik J (2002) Possible ctenophoran affinities of the Precambrian "sea-pen" *Rangea*. *J Morphol* 252:315-334.